Desidero ringraziare:

i miei genitori per essermi stati vicino e per avermi dato l'opportunità di proseguire i miei studi,

gli amici con cui ho passato cinque impegnativi dal punto di vista accademico ma accompagnati dai sorrisi e da momenti indimenticabili,

il professore David Diaz Reigosa e i dottorandi Daniel Fernandez e Cristian Blanco per tutto il loro il tempo che mi hanno dedicato, riaccendendo la passione per l'ingegneria .

University of the study of Padova

DEPARTMENT OF ELECTRICAL ENGINEERING

MASTER'S THESIS

Sensorless Control of a Reluctance Synchronous Machine

Student: Matteo Mattiazzo

Supervisor: Prof. Silverio Bolognani

Co-supervisor: Prof. David Diaz Reigosa

Accademic year: 2014/2015

« Die Mathematik ist die Königin der Wissenschaften »

« La matematica è la regina delle scienze »

Carl Friedrich Gauss

Abstract

This thesis shows how to realize a sensorless control in all speeds range, including the position control for a reluctance synchronous machine. Typically, most of the thesis explain and show hot to realize the sensorless controls with program like Simulink. However in these simulations, the problems that we can find with the implementation of a real control are a lot of and they are not considered. The result is to obtain a great control, which works properly only in the simulations.

However, its main target of the thesis is to explain the development of a real sensorless control, the found problems and how to solve them.

The first Chapter talks of the state of the art about the reluctance synchronous machine and its controls. The second Chapter explains the theory of the reluctance synchronous machine, fundamental to obtain the sensorless controls and theory of the used sensorless controls with the respective simulations. The third and fourth Chapters explain the theory and show the simulations of the high frequency and the model reference adaptive system respectively. In the fifth Chapter it is possible to see the obtained experimental results of the two sensorless methods. The last Chapter talks of the conclusions.

Contents

List of Abbreviations and Symbols

Acronyms	Name
PMSM	Permanent Magnet Synchronous Machine
SPMSM	Superficial Permanent Magnet Synchronous Machine
IPMSM	Interior Permanent Magnet Synchronous Machine
RSM	Reluctance Synchronous Machine
IM	Induction Motor
PM	Permanent Magnet
LPF	Low Pass Filter
HPF	High Pass Filter
BSF	Band Stop Filter
P	Proportional
PI	Proportional and Integral
FFT	Fast Fourier Transformed
HF	High Frequency
MBST	Model Based Sensorless Control
MRAS	Model Reference Adaptive System
MTPA	Maximum Torque Per Ampere
PLL	Phase Lock Loop
PWM	Pulse With Modulation

DSP	Digital Signal Processor
IGBT	Insulated Gate Bipolar Transistor
EV	Electric Vehicle

1 Introduction

1.1 Background

Actually, fossil fuels are the primary source of energy on all the world. However, they are limited and in the future they will disappear. Moreover, they are causing a lot of problems with the pollution; about this problem, the most famous fossil fuel is the carbon. Its combustion makes carbon dioxide (CO_2), which causes serious problem on greenhouse effect and on health of the people. Governments introduces new taxes with the target to limit its consumption, but in this mode the energy price was increased.

With the target to solve these problems, removable energy sources were developed. Actually, wind and solar energy are the most developed and commercially used renewable energy sources. The electrical machines are used in industry and civil field, an estimated 65% of the electrical energy is consumed by electrical motor and the production of the electrical energy is realised with generators, so it is important to develop them with a high efficiency and a great control.

1.2 The Reluctance Synchronous Machine

The permanent magnet synchronous machines (PMSMs) are a lot of used, especially for the production of energy by wind, on the electric vehicle (EV) and in the industries. This type of electrical machine is a valid alternative at the induction machine (IM), thanks to their performance, like efficiency and torque.

Another type of synchronous machine is become import: the synchronous reluctance machine (RSM). It was invented by Danielson in 1900s with the target to improve the power factor respect the IM. For this motivation the SRM, at the first time, was called self-starting synchronous machine, because it can start alone and works at the synchronous speed. Initially the RSM, respect the IM, had only a different rotor, which had a new magnetic saliency, made with the removal of some teeth. This type of motor found utilization in the textile industry.

Only in the 1980s the RSM attained importance thanks to T. A. Lipo, that wrote a paper, intituled “Synchronous Reluctance Machine – A variable Alternative for AC Drives”, where he explained how to develop a better current control and rotor design.

Actually, the RSM has a non-salient three –phase stator and a rotor with a magnetic anisotropic without windings, indeed all these type of electrical machines are called also brushless machines.

Advantages of the RSMs:

- They have a bigger reliability than PMSMs, because they have not permanent magnet and there is not the possibility to demagnetize them with a high current or temperature.

- They have a 15% larger torque density respect IMs.

- Their efficiency is bigger than IMs efficiency.

- They have not brushes or slip-ring.

- Maintenance and costs are low.

- The rotor has a lower inertia and it is light.

- It is possible to estimate the rotor position, developing a position sensorless control, in the PMSM this isn't possible without the ringed pole technique.

- Absence of the cogging torque.

Disadvantages of the RSMs:

- The PMs (permanent magnets) give an important contribution at the torque, so in the RSMs the specific power and the torque density are lower respect the PMSMs.

- The saturation effects of the magnetic circuit are heavy.

1.3 Structure of the control

1.3.1 Sensored control

The structure of the control is reported in the Fig. 1:

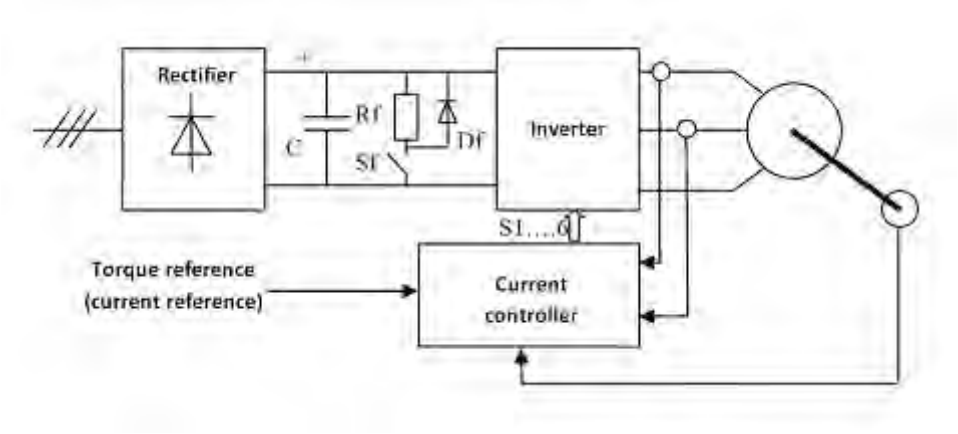

Figure 1: typical electric control with encoder

From the source, typically a three-phase line, it is obtained a direct voltage (V_{DC}) thanks to a rectifier realized with uncontrolled diodes. The DC voltage is applied a three-phase inverter and its control is given by current control. To obtain a good control, it is necessary to know speed and position of the rotor. The currents are obtained with the measure of two currents by transducers, the third current is obtained using the Kirchhoff law, like sum the two measured current, but with the opposite sign.

On the DC line, there is a capacitor with the target to keep a constant voltage and a system to dissipate the braking energy, it is realised with a braking resistance R_f, connected directly to the positive point of the DC line and with a switch to the negative point. This switch is closed when the line voltage is higher than voltage limit and it is opened when the line voltage has a value smaller than voltage limit value.

1.3.2 Sensorless control

Development of the sensored control is completed, with this type of control the obtained performance are amazing and however a sensor has some disadvantages:

- It has a high price.
- It can be broken.

- Impossibility of its use in particular condition.

The general structure of the control is shown in the Fig. 2.

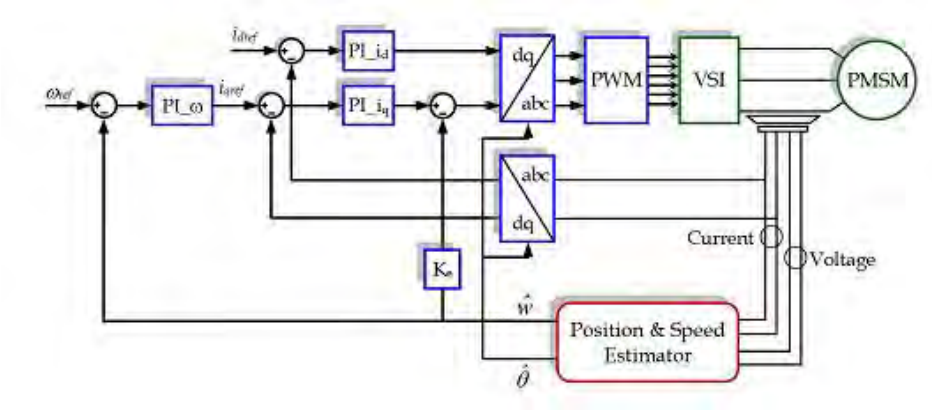

Figure 2: traditional sensorless electric control

For these motivations, the development and research of the sensorless control is become very important. This thesis develops the HF (high frequency) method for the low and zero speed sensorless control and the MRAS (model reference adaptive system) method for the medium and high speed sensorelss control.

The main target of the thesis is to show how to realize a sensorless control in all speed range.

2 . Reluctance synchronous machine and its control

2.1 Introduction

To control a RSM, before it is important to understand how it works, so the first part of the Chapter talks about of the RSM model and of its optimal control. In the second part of the Chapter it is explained how the current, speed and position controls function and how their parameters are calculated.

2.2 RSM model

To develop all type of control it is needful to know the RSM functioning and to get the equations to describe it. All the type of controls, sensored and sensorless are based on this study.

The brushless machines can be grouped in three categories:

- Surface permanent magnet synchronous machines (SPMSMs): they have the PMs on the rotor surface which has not a magnetic anisotropy, given the d and q inductances with the same values.

- Interior permanent magnet synchronous machines (IPMSMs): the PMs are placed in the cavity of the rotor, making a magnetic anisotropy, so the d and q inductances have a different values.

- Reluctance synchronous machine: they have not the PMs and the magnetic anisotropy is made with a specific rotor design, given the d and q inductance result to have a different values.

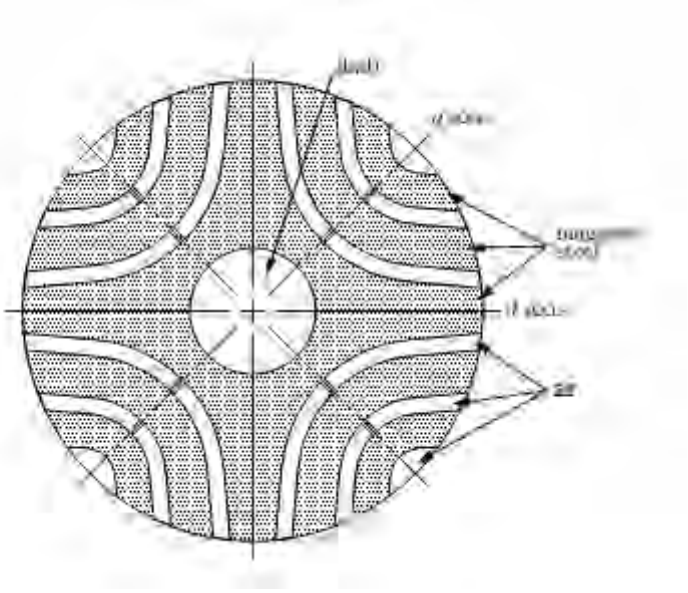

Figure 3: design of the RSM rotor

The RSM is modelled in the stationary synchronous reference frame in the following way. The voltage equation results:

$$v_{dq}^{s} = Ri_{dq}^{s} + L\frac{di_{dq}^{s}}{dt}$$

where R is the stator resistance and $L = L_{ss} + |L_{Mss}|$ is the synchronous inductance, L_{ss} is the auto-inductance and L_{Mss} is the mutual-inductance. With the separated axes:

$$v_{d}^{s} = Ri_{d}^{s} + L_{d}\frac{di_{d}^{s}}{dt}$$
$$v_{q}^{s} = Ri_{q}^{s} + L_{q}\frac{di_{q}^{s}}{dt}$$

Obtaining:

$$\begin{bmatrix} v_d^s \\ v_q^r \end{bmatrix} = R\begin{bmatrix} i_d^s \\ i_q^s \end{bmatrix} + \frac{d}{dt}\begin{bmatrix} \sum L + \Delta L\cos(2\theta_r) & \Delta L\sin(2\theta_r) \\ \Delta L\sin(2\theta_r) & \sum L + \Delta L\cos(2\theta_r) \end{bmatrix}\begin{bmatrix} i_d^s \\ i_q^s \end{bmatrix}$$

where θ_r is the electric position of the RSM rotor. $\sum L$ and ΔL are respectively the average inductance and differential inductance, they are calculated with the following equations:

$$\sum L = \frac{L_d + L_q}{2}$$
$$\Delta L = \frac{L_q - L_d}{2}$$

To obtain the rotating reference frame with the same speed of the rotor (called synchronous reference frame), the following matrices are necessary, given by the Prank transformation:

$$T_{s\to r} = \begin{bmatrix} \cos(\theta_r) & \sin(\theta_r) \\ -\sin(\theta_r) & \cos(\theta_r) \end{bmatrix}$$
$$T_{r\to s} = \begin{bmatrix} \cos(\theta_r) & -\sin(\theta_r) \\ \sin(\theta_r) & \cos(\theta_r) \end{bmatrix}$$

The voltage equations in the synchronous reference frame result:

$$v_d^r = Ri_d^r + L_d \frac{di_d^r}{dt} - \omega_{me} L_q i_q^r$$
$$v_q^r = Ri_q^r + L_q \frac{di_q^r}{dt} + \omega_{me} L_d i_d^r$$

L_d and L_q are the inductances of the d and q axes respectively.

The electric power results:

$$P_e = \frac{3}{2}\left(v_d^r i_d^r + v_q^r i_q^r\right)$$

And the torque results:

$$m = \frac{P_e}{\omega_{me}} = \frac{3}{2} p\, i_q^r\, i_d^r \left(L_d - L_q\right)$$

where ω_{me} is the electric rotor speed and p is the pole pairs. The torque is given only by the reluctance torque, so to increase the torque density, the RMS needs a high saliency ratio ϵ.

$$\epsilon = \frac{L_d}{L_q}$$

Fig. 4 shows the RSM model in the synchronous reference frame:

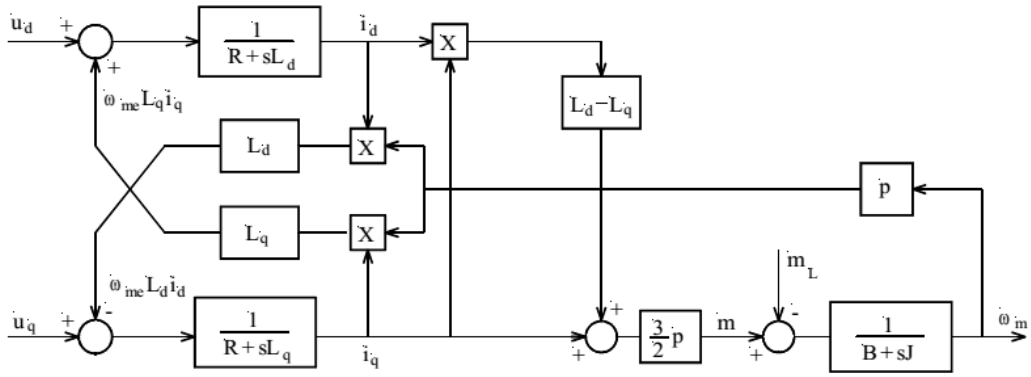

Figure 4: RSM model in rotating reference frame

From now on, the equations will always be reported to the synchronous reference frame, so the rotation reference apex will not be used until the end of the report.

However, current and voltage are limited by the speed and torque limits:

$$i_d^2 + i_q^2 \leq I_n^2$$
$$v_d^2 + v_q^2 \leq V_n^2$$

where I_n is the maximum value of the stator current (it is possible to use a higher current only for short time, taking advantage of the rotor thermic inertia) and V_n is the maximum value of the stator voltage, given by the isolation class of the stator wiring.

The current limit equation, in the I_d/I_q plan, represents a circumference with the centre on the origin. Neglecting the resistance and assuming to be in steady state, the voltage equations became:

$$V_d = -\Omega_{me} L_q I_q$$
$$V_q = \Omega_{me} L_d I_d$$

Replacing them in the voltage limit equation:

$$V_d^2 + V_q^2 = \left(-\Omega_{me} L_q I_q\right)^2 + (\Omega_{me} L_d I_d)^2 \leq V_n^2$$

the last equation becomes:

$$\left(\frac{L_q I_q}{L_d}\right)^2 + I_d^2 \leq \left(\frac{V_n}{\Omega_{me} L_d}\right)^2$$

This equation, in the I_d/I_q plan, represents an ellipse whose centre has the coordinates $I_{Cd} = 0;\ I_{Cq} = 0$.
These currents are also the short-circuit currents of the motor in rotation. The ellipse form changes with the rotation speed: when the speed increases, the area of the ellipse decreases.

The torque equation, written with the q current in function of the other parameters, results:

$$I_q = \frac{2M}{3pI_d\left(L_d - L_q\right)}$$

It's a hyperbole with the asymptote on the origin. When there is the tangency of the torque line with the current limit circumference, the torque has maximum value. All these points, obtained changing the maxim value of the limit current, are the MTPA (maximum torque per ampere). The MTPA has the purpose to obtain the maximum torque with the minimum current minimizing the losses. The MTPA equation is obtained by the orthogonality of the tangent line with the torque line, with the radius of circumference.

The radius of the circumference is:

$$r_1 = \frac{I_q}{I_d}$$

The tangent of the hyperbolic is obtained in the sequent mode:

$$r_2 = \frac{d}{dI_d} I_q = \frac{-2M}{3p(L_d - L_q)I_d^2}$$

Using the torque equation, we have:

$$r_1 = \frac{I_q}{I_d}$$

The orthogonality condition is:

$$r_1 \perp r_2 \Longrightarrow m_2 = \frac{-1}{m_1}$$

So, in the I_d/I_q plan it becomes:

$$I_q = \pm I_d$$

however, to have low losses, it's needed a negative d current. To obtain a positive torque, the q current value must be negative.

$$I_q = I_d$$

In the MTPA, the d and q currents have the same amplitude. Expressing the torque equation with the d and q currents in function of their amplitude and phase, it results:

$$m = \frac{P_e}{\omega_m} = \frac{3}{2} p\, I^2 \sin(\alpha) \cos(\alpha) \left(L_d - L_q\right)$$

where α is the angle of the vector current respect the d axis. Fig. 5 shows the torque waveform in function of this angle.

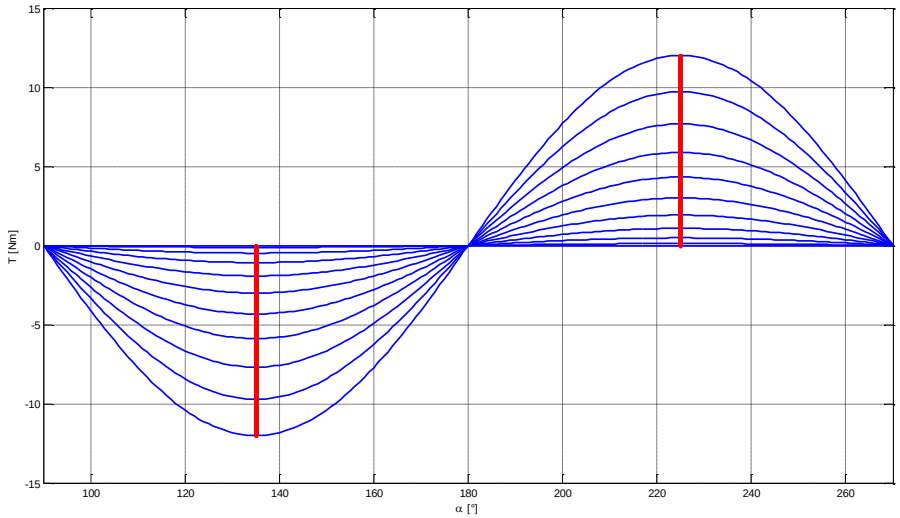

Figure 5: RSM torques in function of the current angle (blue lines) and MTPA (red lines)

Fig. 6 displays the region of operation of the RSM with a positive torque:

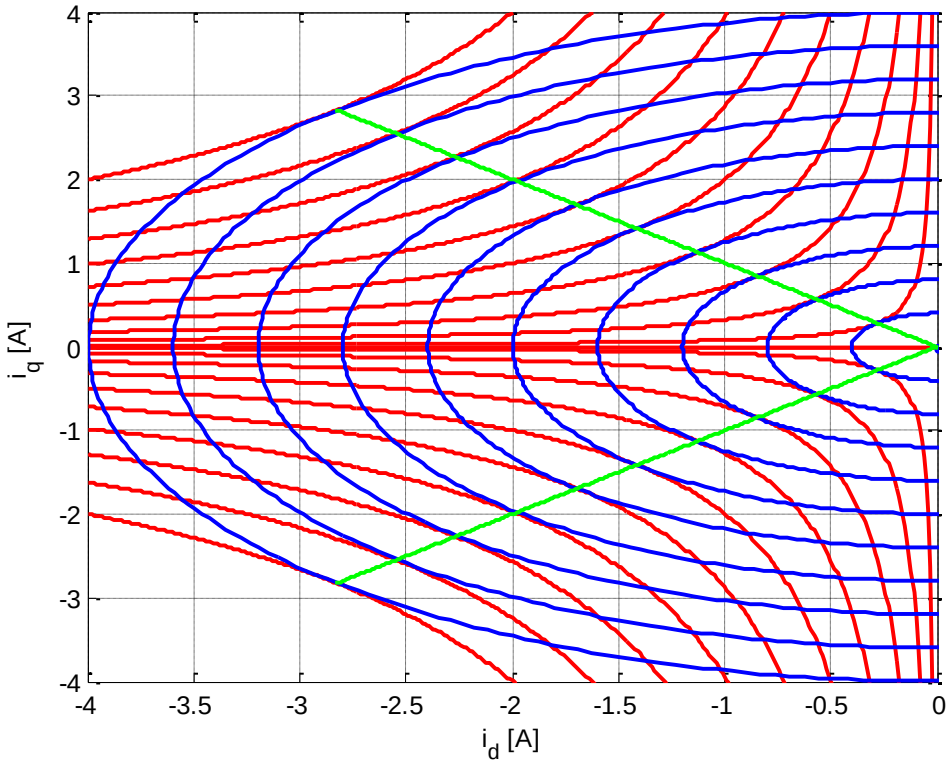

Figure 6: region of operation of the RSM with current limits (blue lines),torque lines (red lines) and MTPA (green lines)

Fig. 6 shows torque and power in function of the electric speed. The area where the torque is constant is the MTPA area, here the RSM can works in the MTPA, with a constant torque until the base speed Ω_B, equal to:

$$\Omega_B = \frac{V_n}{L_d I_n}$$

These speed results lower than synchronous speed.

The following table reports the RSM parameters:

Parameters	Values
Power	1500 W
Nominal torque	9,6 Nm
Nominal speed	1500 rpm
Nominal phase voltage	370 V
Nominal phase current	3,9 A
Pole pairs	2
Stator resistant	3,2 Ω
d axis inductance	0,31 H
q axis inductance	0,10 H

2.3 RSM control

In this section of the Chapter it is described how the current, speed and position regulators are designed. How shown in the Chapter 1, the PWM inverter inputs are the outputs of the current regulators. The current regulators inputs are the errors given by the differences of the reference and measured currents of the axes d and q. With the target to wonk on the MTPA, the d current reference is obtained by the MTPA equation and the q current reference is the output of the speed regulator that its input is the error given the difference of the reference speed with the measured (or estimated) of the rotor. In the case of a position control, the reference speed is the exit of the position regulator and the input of this regulator is the error given by the difference of the reference position with the measured (or estimated) position of the rotor.

2.3.1 Current regulator design

The current transducer used to measure the phase current is a LA 50-P, its transfer function in the Laplace domain results:

$$\frac{I_m(s)}{I(s)} = \frac{k_i}{1 + s\tau_i}$$

where I_m is the measured current and I is the output of the transducer current. It is a function of the first order, where k_i is the gain. The transducer introduces a little delay τ_i, because the reading of the current value and the sending of the signal don't occur in the same time.

The transfer function of the inverter in the Laplace domain is:

$$\frac{V_m(s)}{V(s)} = \frac{k_c}{1 + s\tau_c}$$

where k_c is the gain and τ_c is the delay introduced by the PWM inverter controller that has to split a period in many smaller fraction, creating a square control waveform signal. Therefore the resulting signal has a square wave form and the inverter controller needs time to execute all this.

The block model results:

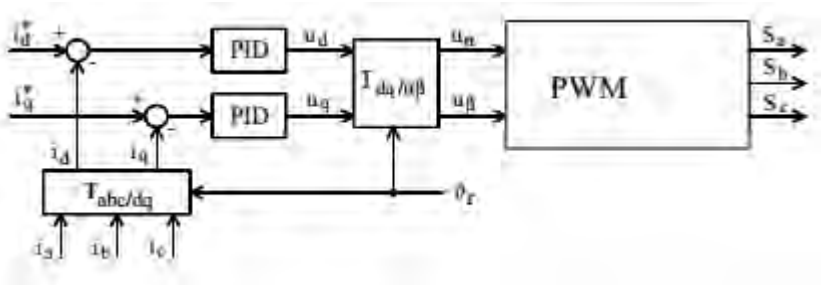

Figure 7: current control model

The function block of the Laplace transformation can be modified in the follow way:

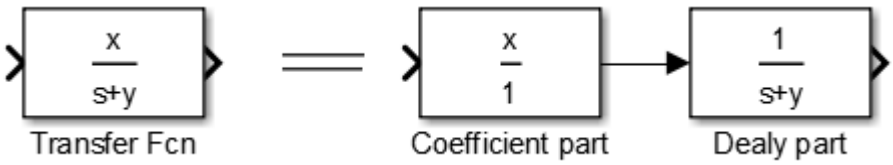

Figure 8: propriety of the Laplace trasformation

This propriety is applied to the block of the inverter and of transducer. Afterwards, the input signals of the node $i_{ref} - i_m = \varepsilon_i$ are divided to the gain of the current transducer, eventually the output signal is multiplied to the gain of the current transducer.

The transducer LA50P introduces a very small delay, so it can be neglecting and thanks to the property of the Laplace function, the obtained control has a close loop with a unitary reaction. Then, the gains k_i and k_c are englobed in the current regulator block.

Since the system works with complex values, explicating the real and imaginary parts, these observations can be decocted:

- The d and q controls are independent.

- The d and q blocks of the RSM are dependent, due to a product between variables from the two different axis. For this reason the RSM model is not linear.

To solve this problem it is necessary to uncouple the two axes. This can be done, neglecting the inverter delay in this case, so the $\omega_r L_q I_q$ and $-\omega_r L_d I_d$ signals are added to the outputs of the current regulators of the d and q axes respectively.

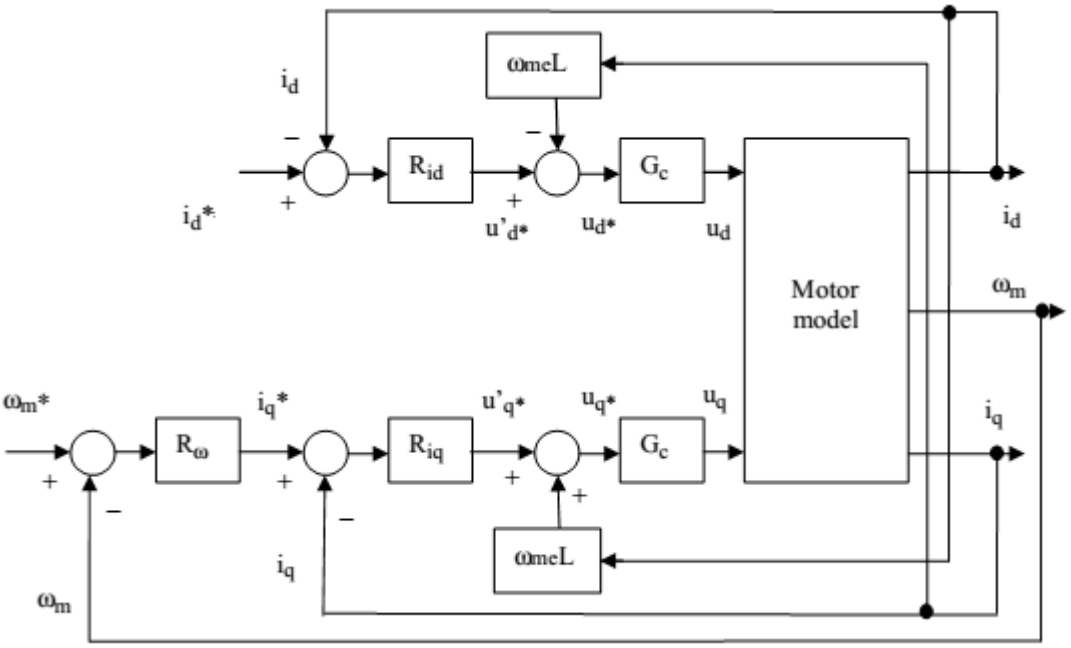

Figure 9: diagram blocks of the RSM and its control

Now the d and q axes are uncoupled so they are studied separately. In the RSM control, the control structure of the d and q axis is the same. The block diagram is approximated like in the Fig. 10:

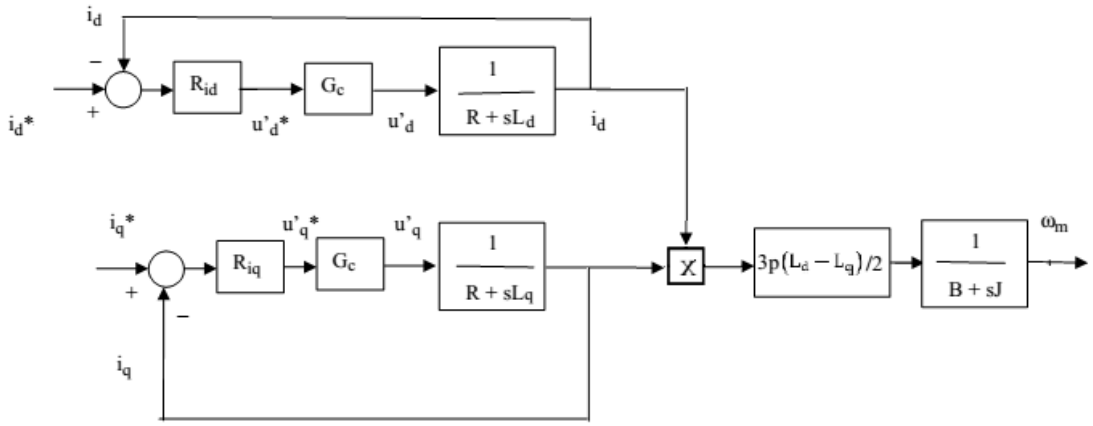

Figure 10: model of the RSM and its current control

The project of the current regulator is conducted to achieve a specific performance that are expressed by:

- Current error in steady state $\epsilon_{i\,d,q}(\infty)$ with a step input.

- Current error in steady state $\epsilon_{i\,d,q}(\infty)$ with a noise torque.

- Bandwidth $f_{BW\,id,q}$: it is measured in Hertz and it is the maximum frequency of a signal reference followed that the regulator follows with a little error. More the bandwidth is bigger and more the rise time is higher.

- Phase margin $\varphi_{m\,i\,d,q}$: it is measured in degree and it affects the stability of the system and its overshot. More the phase margin is bigger and more the system is stable and the overshot is lower.

The design of the regulator is based on the Bode diagrams.

To control the RSM are used PI (proportional and integral) regulators:

$$R_{i\,d,q} = K_{P\,i\,d,q} + \frac{K_{I\,i\,d,q}}{s}$$

where $K_{P\,i\,d,q}$ and $K_{I\,i\,d,q}$ are respectively the proportional gain and the integral gain.

The technique based on Bode diagram requires the frequency study of the of the open loop function GH, where G is the function of the transfer function and H is the function of the feedback, that in this is case is equal to one.

The project starts with the study of the open loop system without regulator GH_R, it results:

$$GH_R = \frac{1}{(1+s\tau_c)(R+sL_{d,q})} = \frac{1}{R(1+s\tau_c)(1+s\tau_{e\,d,q})}$$

The output is a complex number, it gives two information: the module of the ratio and the phase difference between output and input signals of the block. The transfer function in the frequency study is:

$$GH_R(j\nu) = \frac{1}{R(1+j\nu\tau_c)(1+j\nu\tau_{e\,d,q})}$$

where ν is the frequency.

Il Bode diagrams are a logarithmic diagrams, the module becomes $20Log(|input|)$ and decreases or increases to 20 $\frac{dB}{decade}$ for every pole or zero. When the imaginary or the real part is lower of the other part, this last can be neglected

Usually, the inverter constant time is lower than the electric constant time.

- If $\nu < \frac{1}{\tau_{e\,i\,d,q}} < \frac{1}{\tau_c}$ it is like to obtain $GH_R(j\nu) = \frac{1}{R}$
- If $\frac{1}{\tau_{e\,i\,d,q}} < \nu < \frac{1}{\tau_c}$ it is like to obtain $GH_R(j\nu) = \frac{1}{R(j\nu\tau_{e\,d,q})}$
- If $\frac{1}{\tau_{e\,i\,d,q}} < \frac{1}{\tau_c} < \nu$ it is like to obtain $GH_R(j\nu) = \frac{1}{R(j\nu\tau_{e\,d,q})(j\nu\tau_c)}$

It is necessary to use a PI regulator, because with only a P regulator introduces a constant error in steady state. To have a stable system, a phase margin should be equal or higher than 45 degrees. To obtain this, the bandwidth cannot be higher than the inverse of the inverter time constant.

The transfer function of a PI regulator can be written in the follow form:

$$R_{i\,d,q} = \frac{K_{I\,i\,d,q}\left(1 + s\tau_{PI\,i\,d,q}\right)}{s}$$

where $\tau_{PI\,i\,d,q} = \frac{K_{P\,i\,d,q}}{K_{I\,i\,d,q}}$ is constant time of the PI regulator
Its Bode diagram is:

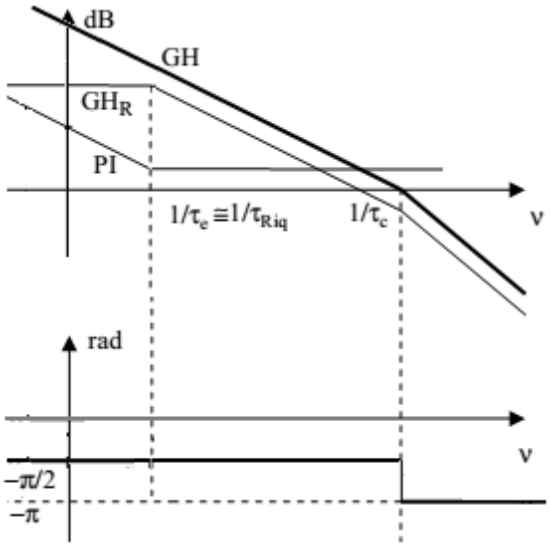

Figure 11: Bode diagram of the current control with PI regulator

With high frequency a PI regulator behaves like a P regulator. The PI regulator has a pole on the origin and this changes the behaviour of the output in the range with low frequencies. The time constant $\tau_{PI\ i\ d,q}$ should have a high value, but it cannot have a value close to inverter constant time. As already mentioned, the principal advantage of the PI regulator is to have an error in steady state equal to zero: the integrator accumulates the errors, increasing its output until the error disappears.

There are two ways to design the regulator:

- **First method:**

In a PI regulator there are two variables to choose and a specific bandwidth and phase margin are required. The open loop transfer function with regulator in the frequency study results:

$$GH(s) = R_{i\ d,q}(j\nu)\ G_c(j\nu)\ \frac{1}{\left(R + j\nu L_{d,q}\right)}$$
$$= \frac{K_{I\ i\ d,q}\left(1 + j\nu\tau_{PI\ i\ d,q}\right)}{j\nu}\ \frac{1}{(1 + j\nu\tau_c)}\ \frac{1}{\left(R + j\nu L_{d,q}\right)}$$

The first step is to calculate the time constant of the regulator with the first performance condition:

$$\angle(GH(jv_{bw})) = -\pi + \varphi_m$$
$$= \tan^{-1}\left(\frac{v_{bw}\tau_{PI\ i\ d,q}}{1}\right) - \left[\frac{\pi}{2} + \tan^{-1}(v_{bw}\tau_c) + \tan^{-1}\left(v_{bw}\tau_{PI\ i\ d,q}\right)\right]$$

The second step is to calculate the integral gain of the regulator with the second performance condition:

$$|GH(jv_{bw})| = 1 = \frac{K_{I\ i\ d,q}\sqrt{1 + \left(v_{bw}\tau_{PI\ i\ d,q}\right)^2}}{v_{bw}\sqrt{1 + (v_{bw}\tau_c)^2}R\sqrt{1 + \left(v_{bw}\tau_{PI\ i\ d,q}\right)^2}}$$

Eventually the proportional gain is obtained:

$$K_{P\ i\ d,q} = \tau_{PI\ i\ d,q} K_{I\ i\ d,q}$$

- **Second method:**

This technique starts imposing regulator time constant equal to the electric time constant, obtaining the elimination of the electric pole, now the transfer function results:

$$GH(s) = \frac{K_{I\ i\ d,q}}{sR(1 + s\tau_c)}$$

The only variable to calculate is the integral gain:

$$|GH(jv_{bw})| = 1 = \frac{K_{I\ i\ d,q}}{v_{bw\ i} R\sqrt{1 + (v_{bw\ i}\tau_c)^2}}$$

Having always $1/\tau_{PI\ i\ d,q} < v_{bw\ i} < 1/\tau_c$, it is possible to neglect the inverter time constant, obtaining:

$$|GH(jv_{bw})| = 1 = \frac{K_{I\ i\ d,q}}{v_{bw\ i} R}$$

However, $K_{P\ i\ d,q} = \tau_{PI\ i\ d,q} K_{I\ i\ d,q}$ and $\tau_{PI\ i\ d,q} = \tau_{e\ d,q}$. It results:

$$K_{P\ i\ d,q} = v_{bw\ i} L_{d,q}$$
$$K_{I\ i\ d,q} = v_{bw\ i} R$$

Eventually it is to verify if the phase margin respects the performance required.

2.3.2 Speed regulator design

For the speed control is always used a PI regulator, its design is very similar to the current regulator design. The block model of the speed control results:

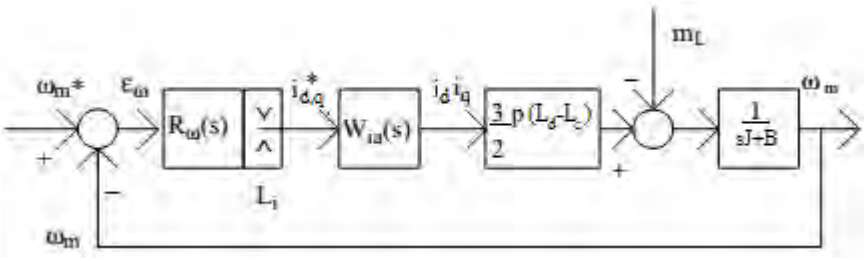

Figure 12: speed control model of the RSM

Primarily, it is hypothesized the load torque is equal to zero. To have a speed control that works properly, the current regulator must be faster, so it is steady state respect the speed control and with a phase margin equal to ninety degrees.

There are different methods to calculate the speed bandwidth speed, but working with the sensorless control, it is chosen ten times lower respect the bandwidth od the speed regulator, In this mode, during the study of the open loop transfer function of the speed control, the d and q currents parts are considered in steady state, namely the blocks became an unitary block. Now the open loop transfer function results:

$$GH(s) = \frac{K_{I\,\omega}(1 + s\tau_{PI\,\omega})}{s} \frac{3p(L_d - L_q)}{2} \frac{1}{B + sJ}$$

How develop for the current regulator, it is used the deletion pole method, imposing the mechanic and speed regulator time constants equal to each other, obtaining:

$$GH(s) = \frac{K_{I\,\omega}}{s} \frac{3p(L_d - L_q)}{2} \frac{1}{B}$$

Now, knowing the speed regulator bandwidth, it is calculated the integral gain:

$$K_{I\,\omega} = \frac{2Bv_{bw\,\omega}}{3p(L_d - L_q)}$$

Remembering that $K_{P\,\omega} = \tau_{PI\,\omega} K_{I\,\omega}$ and $\tau_{PI\,\omega} = \tau_m$, it results:

$$K_{I\,\omega} = \frac{2Jv_{bw\,\omega}}{3p(L_d - L_q)}$$

2.3.3 Position regulator design

To obtain a position control, it is used a P (proportional) regulator, its equation in Laplace domain is:

$$R_\theta = K_{P\,\theta}$$

where $K_{P\,\theta}$ is the proportional coefficient of the position regulator.

Theoretically, it is not necessary a PI regulator. The bandwidth is chosen ten times lower than speed bandwidth, so the proportional coefficient results:

$$K_{P\,\theta} = v_{bw\,\theta}$$

3 . High frequency injection method

3.1 Introduction

The high frequency method is an incredible technique, with the right knowledge it allows to estimate speed, position and temperature of the electrical machine. Saliency tracking-based sensorless control methods use various forms of high frequency (HF) injection to estimate rotor speed and rotor position. Essentially, there are two important types of techniques: rotating vector and pulsating vector.

Rotating vector method injects a balanced three-phase voltage or current carrier signal, making a rotating vector. The responses of the machine are phase-modulated by the magnetic saliency position, the rotor position is estimated from these responses.

Pulsating vector method injects a voltage or current carrier signal only on the estimated d or q axis and the position is found with the minimization of the amplitude of the response signal measured on the axis orthogonal at the injection axis.

All two methods can work with the injection of a voltage or current vector, anyway, it is preferred to inject a voltage signal and to measure the carrier current to find the rotor angle. In an ideal case, these methods work properly, in a real machine there are some problems. For example, saturation and cross-saturation effects introduce an error on the estimation of the angle. There are also problems introduced to dead-time of the inverter and other its problems given by the fact that they are not ideal. In some papers is written that the pulsating method could be less affected by this problem. The pulsating method results more accurate but the rotating method is more robust, so the chosen method is rotating vector carrier signal injection.

The HF voltage is injected on the stator, superimposed on the fundamental voltage

3.2 High frequency method theory

This chapter explains the theory of the high frequency method, based on the injection of a carrier signal, how it is used to estimate the electric rotor position and the position and low speed sensorless control.

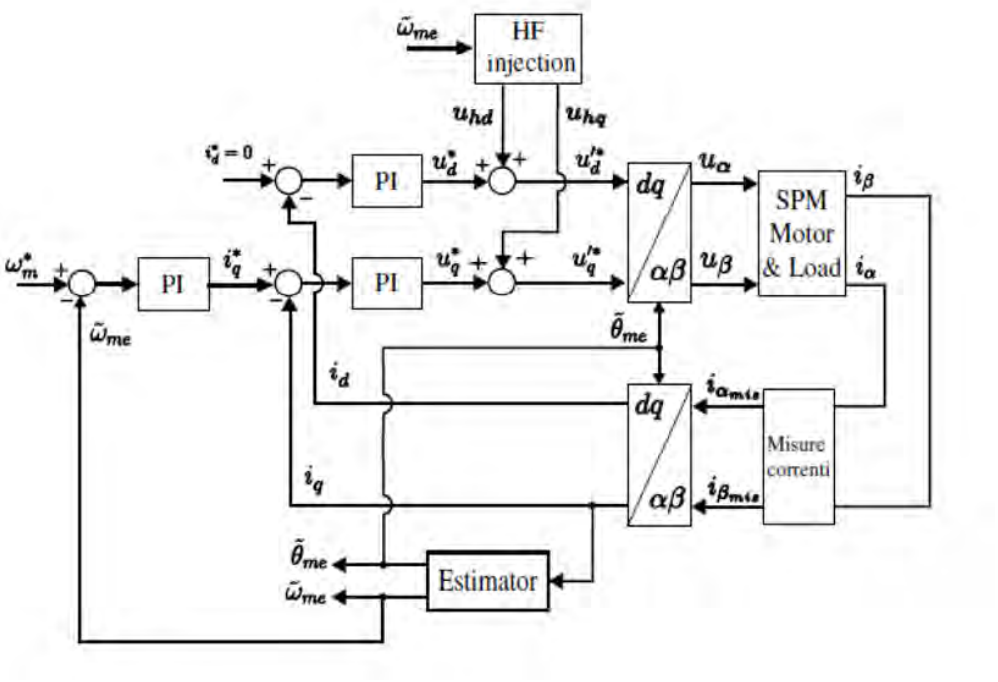

Figure 13: HF injection model

In this part of the chapter the theory of the high frequency injection method will be shown and developed. With this method, a high frequency rotating carrier voltage is injected in the motor also together the fundamental component. The injected voltage has a magnitude V_{hf} and a frequency ω_{hf}. The criterions to choose their values are the following:

- **Frequency selection**

  The switching frequency of the PWM is 10 KHz, and obviously the high frequency cannot have a higher value. With a high frequency of the injected signal, increase the spectral separation with the fundamental excitation frequency and to realize the filters results easier. However, this increases also the impedances given by the inductances and the signal with the rotor information has a smaller magnitude. If it is too low, to obtain the information becomes difficult. In this project, after several attempts, the high frequency is chosen equal to 166 Hz. With this value, the phase of the machine high frequency impedance is, more or less, 81 degrees. In this condition, the resistive component can be neglected.

- **Magnitude selection**

  Increasing the high frequency voltage magnitude, also the signal with the spatial information has a higher magnitude and to read it results easier.

Anyway, with a magnitude too elevate, the machine losses increase, causing noise and vibration. In this job, the magnitude is 150 V, making a high frequency current equal to 0,14 pu.

In the RSM there is a sizable difference in the inductances of the d and q axes, this can be used to estimate the electric rotor position, thanks to the rotating or pulsating vector injection method.

In the first part of the chapter is shown the estimation of the rotor position. In the second part is shown the low speed sensorless control. In the third part is shown the position sensorless control.

Remind the model of the RSM, shown in the chapter 2, the inductances of the d and q axes change due to the magnetic saturation. This change can be modelled with the Taylor series expansion in function of the current, neglecting the cross saturation, because its magnitude is small.

$$L_d = L_{d0} - L_d{}' i_{ds}^r - L_d{}'' {i_{ds}^r}^2$$
$$L_q = L_{q0} - L_q{}' i_{qs}^r - L_d{}'' {i_{qs}^r}^2$$

where $L_d{}' = \frac{dL_d}{di_{ds}^r}$, $L_d{}'' = \frac{d^2L_d}{(di_{ds}^r)^2}$, $L_q{}' = \frac{dL_q}{di_{qs}^r}$ and $L_q{}'' = \frac{d^2L_q}{(di_{qs}^r)^2}$.

Due to this fact, it is better to reason with the reluctance, defining the current like a variable in function of the product of the reluctance with the flux.

$$i_{dqs}^r = \mathcal{R}_{d0}\Delta\lambda_{ds}^r + \mathcal{R}_d{}'\Delta{\lambda_{ds}^r}^2 + +\mathcal{R}_d{}''\Delta{\lambda_{ds}^r}^3 + j\left(\mathcal{R}_{q0}\Delta\lambda_{qs}^r + \mathcal{R}_q{}'\Delta{\lambda_{qs}^r}^2 + +\mathcal{R}_q{}''\Delta{\lambda_{qs}^r}^3\right)$$

with $\Delta\lambda_{ds}^r = \lambda_{ds}^r$ and $\Delta\lambda_{qs}^r = \lambda_{qs}^r$.

$$\mathcal{R}_{d0} = \frac{1}{L_{d0}}, \mathcal{R}_d{}' = \left.\frac{d\mathcal{R}_d}{d\lambda_{ds}^r}\right|_{\lambda_{ds}^r=0}, \mathcal{R}_d{}'' = \left.\frac{d^2\mathcal{R}_d}{d{\lambda_{ds}^r}^2}\right|_{\lambda_{ds}^r=0}$$
$$\mathcal{R}_{q0} = \frac{1}{L_{q0}}, \mathcal{R}_q{}' = \left.\frac{d\mathcal{R}_q}{d\lambda_{qs}^r}\right|_{\lambda_{qs}^r=0}, \mathcal{R}_q{}'' = \left.\frac{d^2\mathcal{R}_q}{d{\lambda_{qs}^r}^2}\right|_{\lambda_{qs}^r=0}$$

A high frequency voltage vector; with a carrier frequency ω_{hf}, is injected in the RSM and in stationary reference frame it results:

$$v_{dqhf}^{s} = V_{hf} e^{j\theta_{hf}} = V_{hf}\left(\cos(\omega_{hf} t) + \sin(\omega_{hf} t)\right)$$

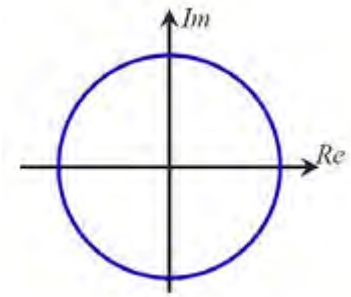

Figure 14: rapresentation of the carrier voltage injected on the RSM

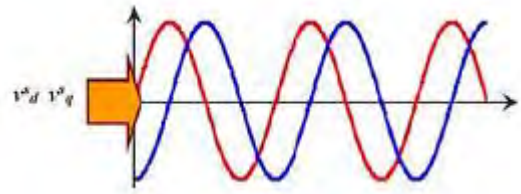

Figure 15: d (red line) and q (blue line) component of the injected voltage vector in the stationary reference frame

The injected voltage consists in a balanced three-phase voltages represented with the following equation and the Fig. 16:

$$v_a = V_{hf} \cos(\omega_{hf} t)$$
$$v_b = V_{hf} \cos\left(\omega_{hf} t - \frac{2\pi}{3}\right)$$
$$v_c = V_{hf} \cos\left(\omega_{hf} t + \frac{2\pi}{3}\right)$$

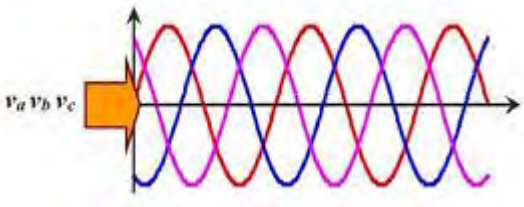

Figure 16: injected voltage vector in three-phase stationary reference frame.

And in the rotor reference frame it is equal to:

$$v_{dqhf}^{r} = v_{dqhf}^{s} e^{-j\theta_r} = V_{hf} e^{j\omega_{hf} t} e^{-j\theta_r} = V_{hf}\left(\cos\left(\omega_{hf} t - \theta_r\right) + \sin\left(\omega_{hf} t - \theta_r\right)\right)$$

An advantage to use the high frequency is to neglect the stator resistance, because the reactance given by the inductance is higher, so from the voltage equation shown in the Chapter 2, it is possible to obtain the frequency stator flux in the rotor reference frame:

$$\lambda_{dqshf}^{r} = \int v_{dqhf}^{r} - R i_{dqhf}^{r} dt \approx \int v_{dqhf}^{r} dt \approx \frac{V_{hf}}{\omega_{hf}}\left(\cos\left(\omega_{hf} t - \theta_r\right) + \sin\left(\omega_{hf} t - \theta_r\right)\right)$$

Replacing this stator flux, the information of the electric rotor position is shown.

$$i_{dqshf}^{s} = I_{hf\,1p} e^{j(\omega_{hf} t + \phi_{1p})} + I_{hf\,1n} e^{j(-\omega_{hf} t - 2\theta_r + \phi_{1n})} + I_{hf\,2p} e^{j(2\omega_{hf} t - \theta_r + \phi_{2p})} + I_{hf\,2n} e^{j(-2\omega_{hf} t + 3\theta_r + \phi_{2n})}$$

Where

$$I_{hf\,1p} = \frac{V_{hf}}{\omega_{hf}} \frac{L_{d0} + L_{q0}}{2 L_{d0} L_{q0}} + \frac{3 {V_{hf}}^3 {\mathcal{R}_d}'}{8 {\omega_{hf}}^3} + \frac{3 {V_{hf}}^3 {\mathcal{R}_q}'}{8 {\omega_{hf}}^3}$$

$$I_{hf\,1n} = \frac{V_{hf}}{\omega_{hf}} \frac{L_{q0} - L_{d0}}{2 L_{d0} L_{q0}} + \frac{3 {V_{hf}}^3 {\mathcal{R}_d}'}{8 {\omega_{hf}}^3} - \frac{3 {V_{hf}}^3 {\mathcal{R}_q}'}{8 {\omega_{hf}}^3}$$

$$I_{hf\,2p} = I_{hf\,2n} = \frac{V_{hf}}{\omega_{hf}} \sqrt{{\mathcal{R}_d}^2 + {\mathcal{R}_q}^2}$$

$$\phi_{1p} = \frac{\pi}{2}$$

$$\phi_{1p} = -\frac{\pi}{2}$$

$$\phi_{2p} = \phi_{2n} = \tan^{-1}\left(-\frac{{\mathcal{R}_q}'}{{\mathcal{R}_d}'}\right)$$

The first term is the positive sequence component and it hasn't the electric rotor position information. The second term is the negative sequence component and it is possible to obtain the information about the electric rotor position from its. The other terms are harmonic parts of the positive and negative sequences. The negative sequence contains the information 2θ.

Anyway, the high frequency methods cannot work with every synchronous machine type:

- If the rotor is isotropic, having $L_d = L_q$, the high frequency current in the complex plane is a circle like the high frequency voltage and the q and q components of the high frequency current have the same magnitude, how shown in Fig. 17 and Fig. 18, so it is not possible to obtain information about the rotor position.

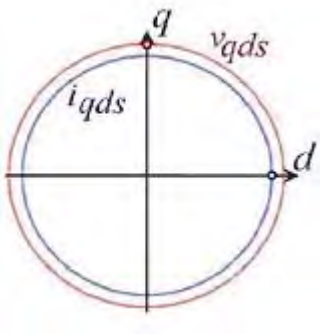

Figure 17: rapresentation of the high frequency vector voltage (red) and the resulting high frequency current vector (blue) with a isotropic rotor

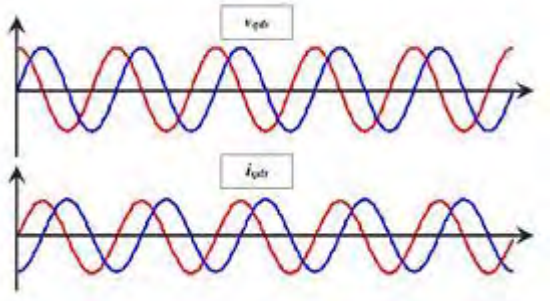

Figure 18: rapresentation of the high frequency vector voltage and the resulting high freqquency current vector with a isotropic rotor with separated d and q components

- In the case with an anisotropic rotor, having $L_d \neq L_q$, the d and q component of the high frequency current are different, in the complex plane the high frequency current is an ellipse with the axis with the higher value oriented in the reference axis with the lower inductance value, because the d and q components of the high frequency current have a different magnitude.

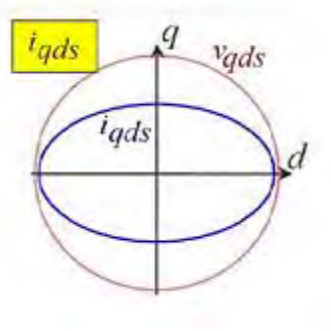

Figure 19: rapresentation of the high frequency vector voltage (red) and the resulting high frequency current vector (blue) with am anisotropic rotor

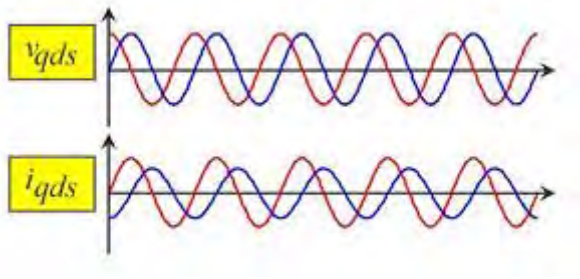

Figure 20: rapresentation of the high frequency vector voltage and the resulting high frequency current vector with an anisotropic rotor with separated d and q components

The spectral components of the injected high frequency voltage and resulting high frequency current for the case of rotating high frequency voltage injection are shown in Fig. 1, spectrum is given in the stationary reference frame.

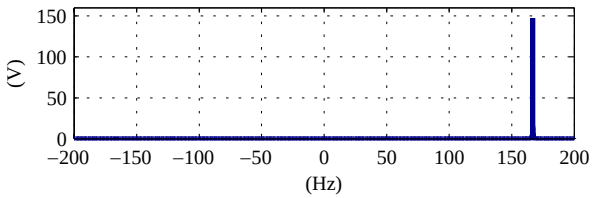

Figure 21: FFT of the injected high frequency voltage

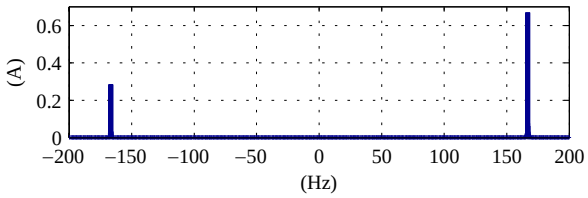

Figure 22: FFT of the high frequency current with an ansitropic rotor

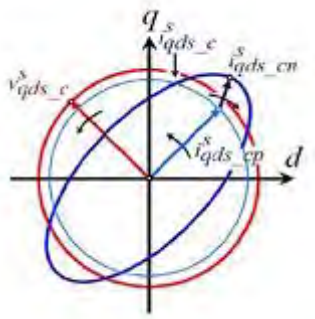

Figure 23: rapresentation of the injected high frequency voltage (red) and of the resulting current (blue) with an anisotropic rotor

To estimate the electric rotor position, it is necessary to isolate the information to the negative sequence component.

During the sensorless control, there is a current formed from the fundamental current and the high frequency current. This part of the chapter shows how the system sunders these two type of current and how the spatial information is obtained.

First, it is indicated how is found the fundamental component of the current, used for the current control.

3.2.1 Isolation of the fundamental current

As known during the steady state, in the synchronous reference frame, the fundamental current has a zero frequency, so it is possible to obtain it using a LPF with a cut-off frequency equal to 10 Hz more or less, or using a BSF with the same frequency of the carrier signal. Anyway, during the transient the fundamental current has also a component with a frequency different to zero and it is important for the current control extract also this component. A LPF introduces a delay for this component and the BSP reduces its magnitude. For these motivation the current fundamental component is gotten with the follow steps:

- **First step**

In the initial situation there are the fundamental component with zero frequency, the positive sequence with a frequency approximately equal to ω_{hf} and the negative sequence with a frequency approximately equal to $-\omega_{hf}$. The target is to eliminate the positive and negative sequences. The first step consists to make a rotation with an angle equal to $-\omega_{hf}t$, in this mode the positive sequence has zero frequency.

- **Second step**

Now the positive sequence is eliminated thanks to a HPF, its frequency mustn't affect the other current components, it is chosen a frequency.

- **Third step**

At present, the new and last target is to eliminate the negative sequence. Therefore it is used another rotation block with an angle equal to $2\omega_{hf}$, changing the frequency of the negative sequence, that now is 0 Hz.

- **Fourth step**

How done in the second step for the positive sequence, the negative sequence is deleted with a HPF.

- **Fifth step**

The last step changes the fundamental current frequency from ω_{hf} at 0 Hz, thanks to a rotation of $-\omega_{hf}t$.

3.2.2 Isolation of the spatial information

The current is composed by the fundamental and high frequency current. To obtain the spatial information, before it is necessary to isolate the negative sequence, this is realized with the following steps:

- **First step**

Using a HPF, the fundamental component is eliminated, the next target it to delete the positive sequence

- **Second step**

It is realized a rotation of the current of an angle equal to $-\omega_{hf}t$, so positive sequence has a frequency equal to zero and the negative sequence frequency is equal to $-2\ \omega_{hf}t$.

- **Third step**

Also done in the first step, the positive sequence is eliminated with a HPF.

- **Fourth step**

  Using another block rotation with an angle equal to 2 $\omega_{hf}t$, the negative sequence has a frequency equal to zero.

- **Fifth step**

Now, it is obtained the negative sequence and with a frequency equal to zero in the rotating reference frame, it results:

$$I_{hf\ 1n}e^{j(-2\theta_r+\phi_{1n})}$$

To give the rotor speed, it is used a PI regulator, where its input is the error given by the imaginary part of the negative sequence, after a rotation equal to ϕ_{1n}. The output of the PI regulator is the electric speed and its integration is the electric angle.

The diagram block for isolation of the spatial information is shown in Fig. 24.

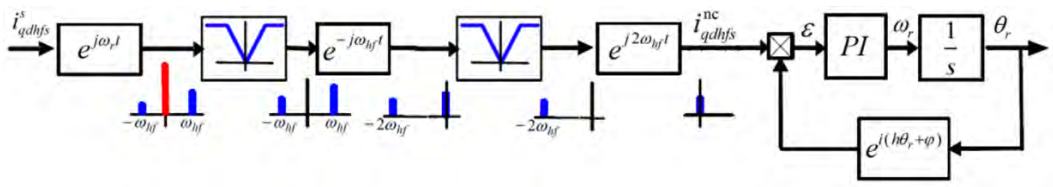

Figure 24: simplified diagram block of the signal processing used for the estimation of the rotor speed and position when using a rotating voltage signal injection

The implementation in Simulink is reported in Fig. 25.

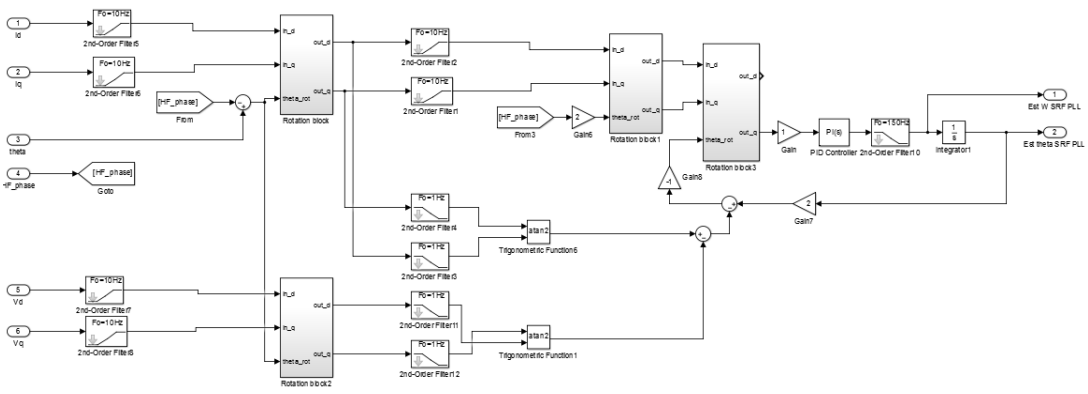

Figure 25: diagram block realized in Simulink to estimate the rotor position

The problem of the filters is the realization of a delay in their outputs, but with this scheme these delays are compensated.

3.3 Simulations of the high frequency method

This part of the Chapter shows the implementation of the simulations of the sensorless control with the HF method. How to explain in the first part of this Chapter, to control a RSM it is necessary before to estimate the position of the d axis, after it is possible to develop a right control.

The program is structured to estimate the rotor position in 2 s, after it is possible to use the current, speed or position sensorless control.

The estimation of the rotor position is very important, also in the MRAS method the electric position is estimated with the HF method at the beginning.

The simulations are realized with Simulink and Matlab 2014a. In all the simulations the solver type is fixed-step, with a step time equal to 1 μs. The PWM inverter is made with the blocks "universal bridge" and "PWM generator" with a frequency equal to 10 kHz. The RSM is represented with the "PM synchronous machine" block.

The method to calculate the gain values of the current and speed regulators is explained in the Chapter 2, the values of the regulators are followings:

Current regulator gains values of the d axis:

$$K_{P\,id} = 15$$
$$K_{I\,id} = 160$$

Current regulator gains values of the q axis:

$$K_{P\,iq} = 5$$
$$K_{I\,iq} = 160$$

Speed regulator gains:

$$K_{P\,\omega} = 0.06688$$
$$K_{I\,\omega} = 0.03344$$

The HPFs, used to separate the fundamental and the high frequency currents have a cut-off frequency equal to 10 Hz. Fig. 26 shows the Bode diagram of the HPFs.

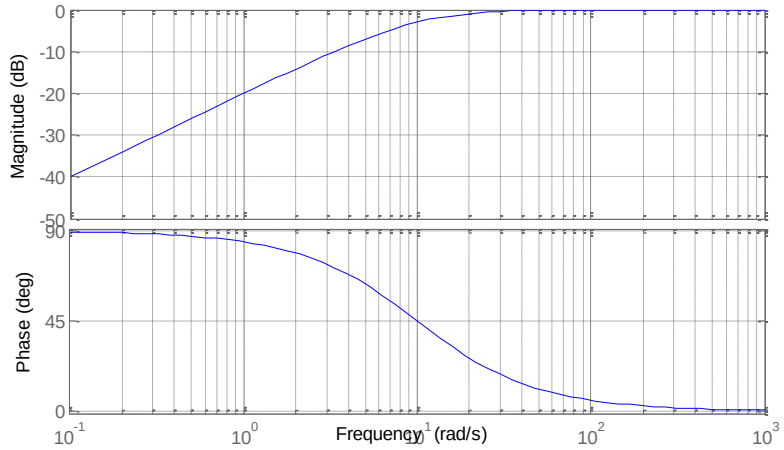

Figure 26: Bode diagram of the HPS with a cut-off frequency equal to 10 Hz

The PLL coefficients are chosen thanks to experimental tests.

$$K_{P\,PLL} = 50$$

$$K_{I\,PLL} = 400$$

3.3.1 Estimation of the angle

The first step is to be sure of the right estimation of the rotor position. In this simulation, the RSM model is supplied with only the HF carrier vector. Imposing a different initial values the rotor position, Fig. shows the performance of the position estimation. It is very fast, in 0,7 s the estimator know the rotor position. There a little constant error that is proportional to the step time, but it is neglecting.

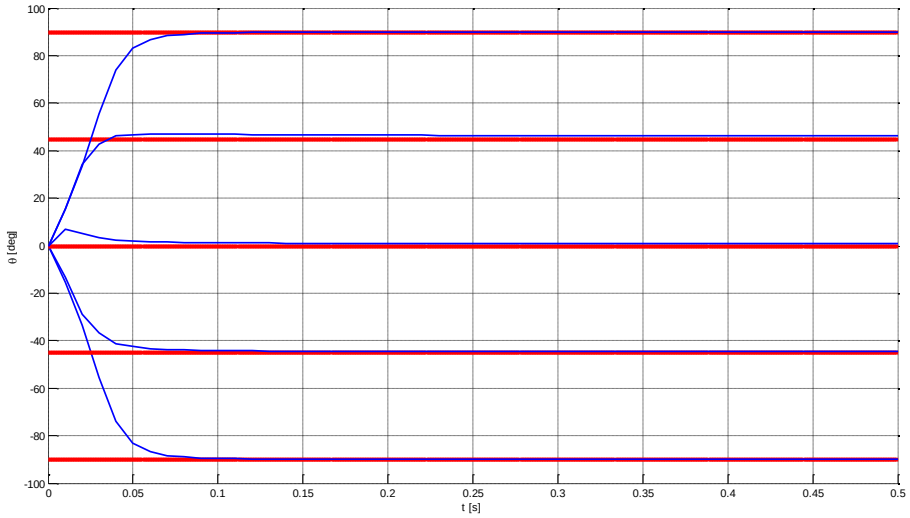

Figure 27: estimated (blue) and actual position (red), after the high frequency voltage is injected, for initial positions of -90, -45, 0, 45 and 90 deg. respectively. Vhf=150 V, ωhf=166 Hz, Iq=0, Id=0, ωr=0 Hz

3.3.2 Estimation of the speed

Next step is to estimate the rotor speed. Also this simulation is realized injecting in the RSM only the HF carrier voltage, imposing the rotor speed with an external source.

Fig. 28 displays the estimated speeds with different reference speed.

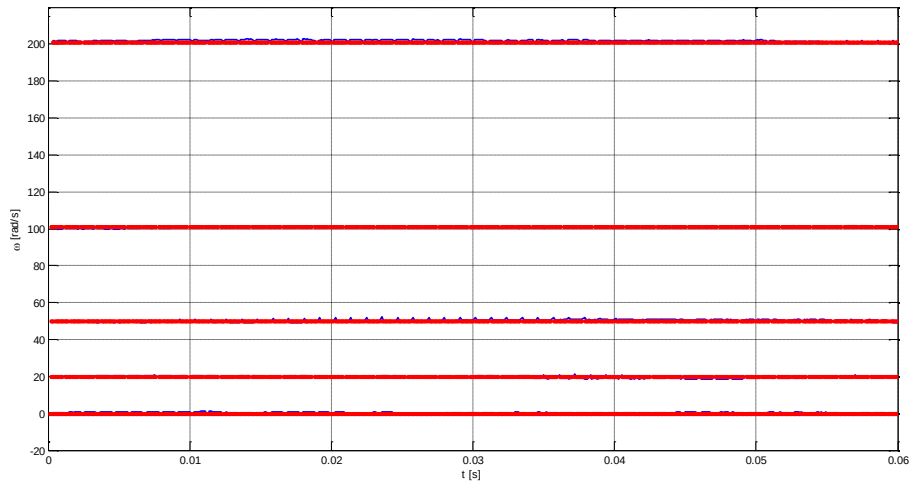

Figure 28: estimated (blue) and measured speed (red), for speeds 0, 20, 50, 100 and 200 rad/s. Vhf=150 V, ωhf=166 Hz, Iq=0, Id=0

Another important test is to use a step speed reference and to observe the estimated speed. This simulation is important to understand the behaviour of the estimator during the speed transient.

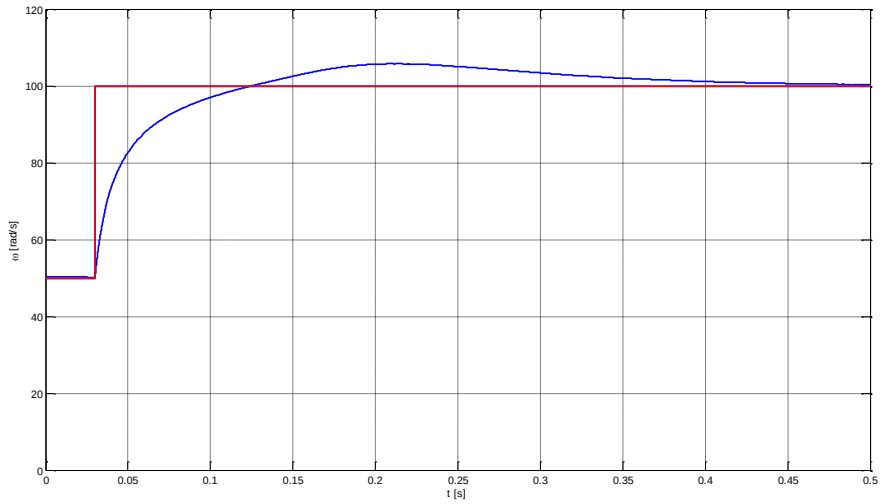

Figure 29: estimated (blue) and measured speed (red) during a speed transient. Vhf=150 V, ωhf=166 Hz, Iq=0, Id=0

Thanks to the obtained results, it is possible to know that the HF estimator works properly.

3.3.3 Current sensorless control by high frequency method

Now, the rotor speed is always imposed with an external source and the RSM is controlled with the current sensorless control. The main problem of this simulation is to split the fundamental current from the HF current, especially during a transient. The control is tested using a step current reference from 0 A until the nominal current. The currents waveforms are shown in Fig. 30.

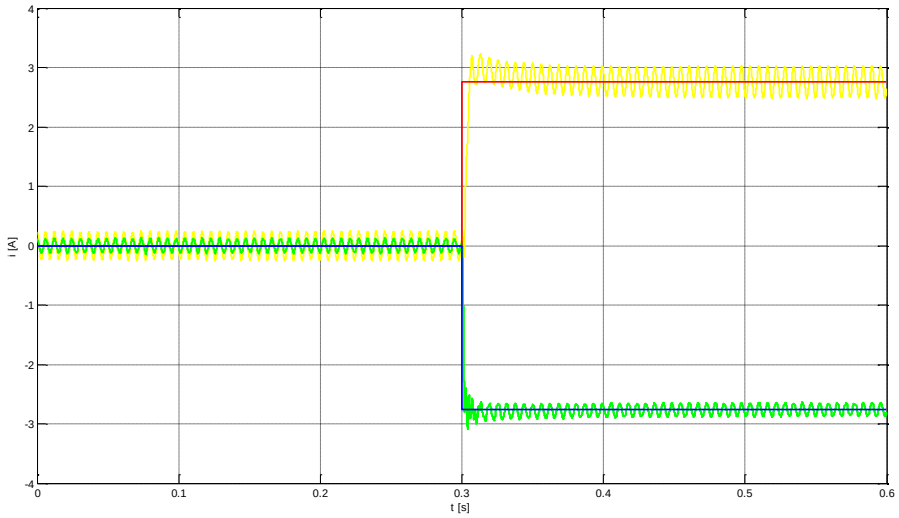

Figure 30: sensorless current control operation. Measured d (blue) and q (red) currents, estimated d (green) and q (yellow) currents. Vhf=150 V, ωhf=2*π*166 Hz, ωr=20 rad/s

Fig. 31 shows the estimated and measured speed of the rotor, how it is possible to see, the estimation, after a very shoet transient, is always right.

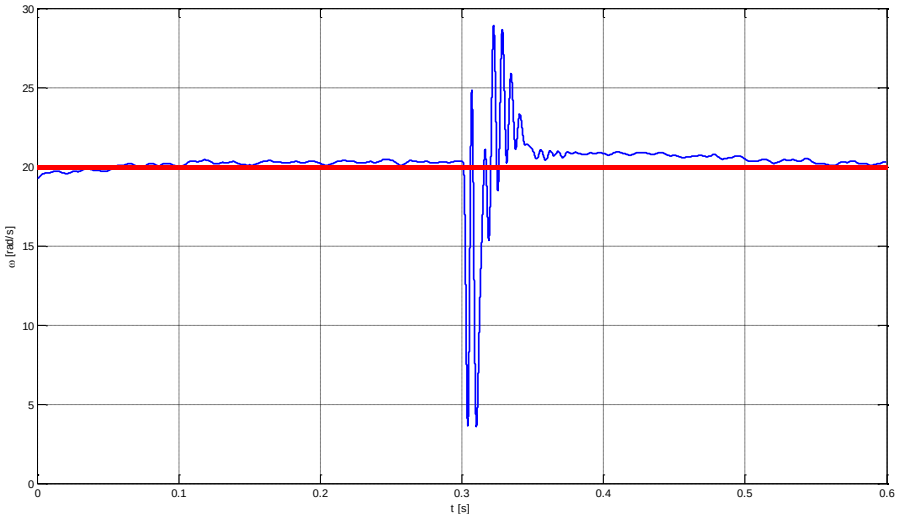

Figure 31: sensorless current control operation. Estimated (blue) and measured (red) speeds. Vhf=150 V, ωhf=2*π*166 Hz, ωr=20 rad/s

During this simulation is also observed the error angle introduced with the step current reference, is it shown in Fig. 32.

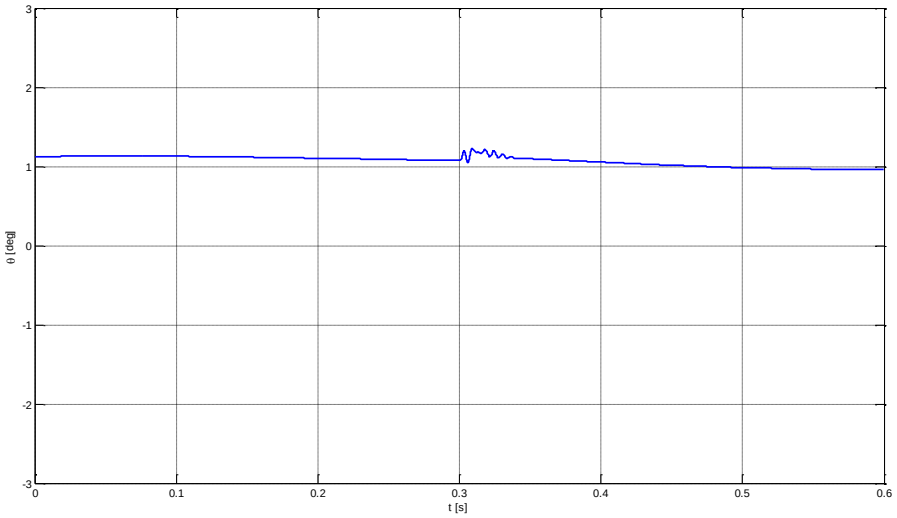

Figure 32: sensorless current control operation. Estimated phase error. Vhf=150 V, ωhf=2*π*166 Hz, ωr=10 rad/s

From the obtained results, it is visible the high performance of the control and that the filters work properly.

3.3.4 Speed sensorless control by high frequency method

Finally the RSM is controlled with the speed sensorless control. The HF method cannot work at high speed, due to the amplitude noise becomes too high, distorting the speed estimator. The method is used to control the RSM with low speed reference, usually this method can work with speed reference equal to 30% to the rated speed. For this motivation the control is tested with a speed reference before equal to 100 rad/s and after equal to -100 rad/s.

Reference speed equal to 100 rad/s

Fig. 33 shows the estimated speed and the measured speed of the RSM with a reference speed equal to 100 rad/s.

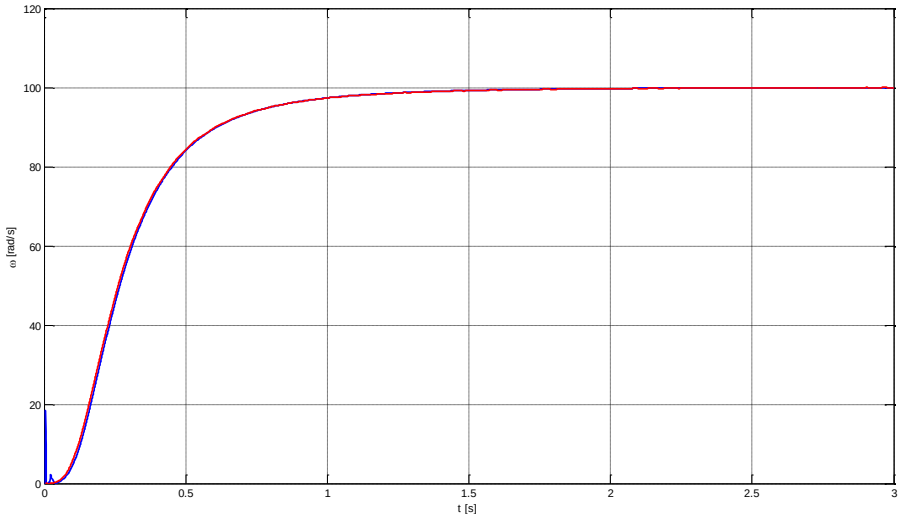

Figure 33: sensorless speed control operation. Estimated and measured speed with a step speed reference equal to 100 rad/s, Vhf=150 V, ωhf=166 Hz

Fig. 34 shows the estimated angle and the measured angle of the RSM with a reference speed equal to 100 rad/s.

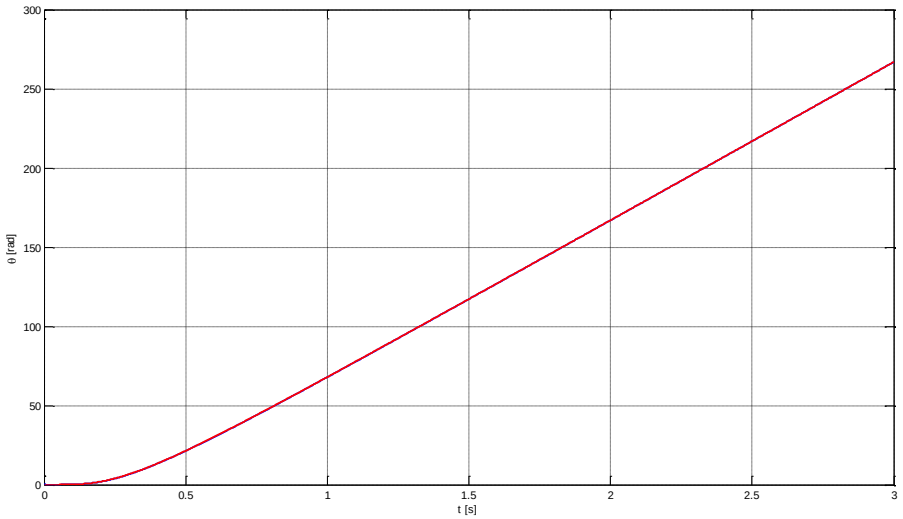

Figure 34: sensorless speed control operation. Estimated and measured angle with a step speed reference equal to 100 rad/s, Vhf=150 V, ωhf=166 Hz

Reference speed equal to -100 rad/s

Fig. 35 shows the estimated speed and the measured speed of the RSM with a reference speed equal to -100 rad/s.

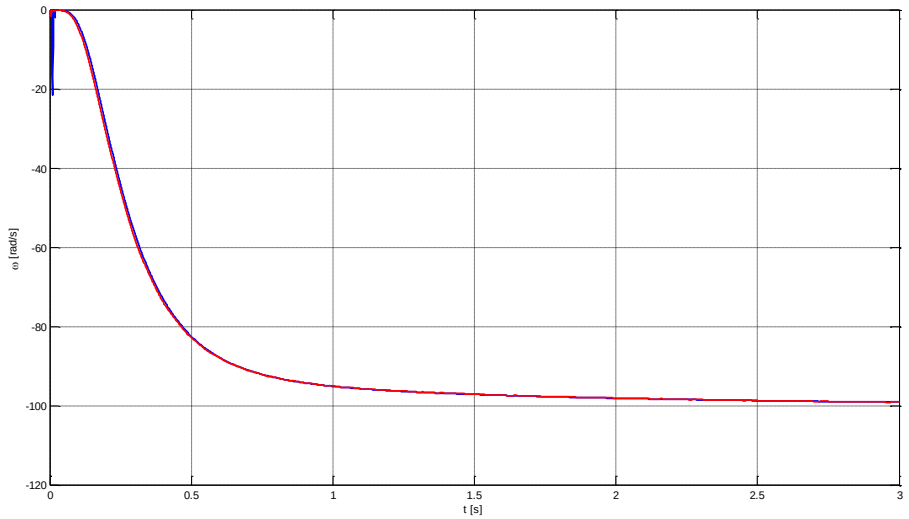

Figure 35: sensorless speed control operation. Estimated and measured speed with a step speed reference equal to -100 rad/s, Vhf=150 V, ωhf=166 Hz

Fig. 36 shows the estimated angle and the measured angle of the RSM with a reference speed equal to -100 rad/s.

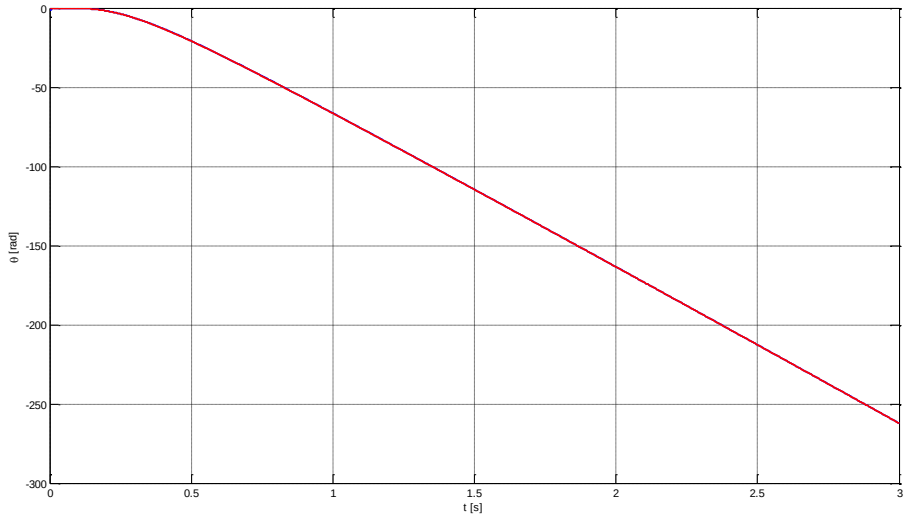

Figure 36: sensorless speed control operation. Estimated and measured angle with a step speed reference equal to -100 rad/s, Vhf=150 V, ωhf=166 Hz

All the simulations have a rise time equal to 1 and there are not overshoots. Thanks to these tests, the speed sensorless control is ready to be implemented for practical experimental.

3.3.5 Position sensorless control by high frequency method

The last simulations are the position sensorless control thanks to the HF technique. To obtain a nice position control it is necessary to have an efficient very low speed increasing the speed bandwidth. For this motivation, the coefficients of the PLL and speed PI regulator, thanks to experimental tests, result:

$$K_{P\,\omega} = 0.8$$

$$K_{I\,\omega} = 0.16$$

$$K_{P\,PLL} = 5$$

$$K_{I\,PLL} = 30$$

Reference position amplitude equal to 35 deg.

Fig. 37 and 38 show the waveform of the position control with a very low reference angle, in this case equal to 35 deg. with respectively a positive and negative reference sign, with an initial position equal to 0 deg. The rise time is 0,3 s and there are not overshoots.

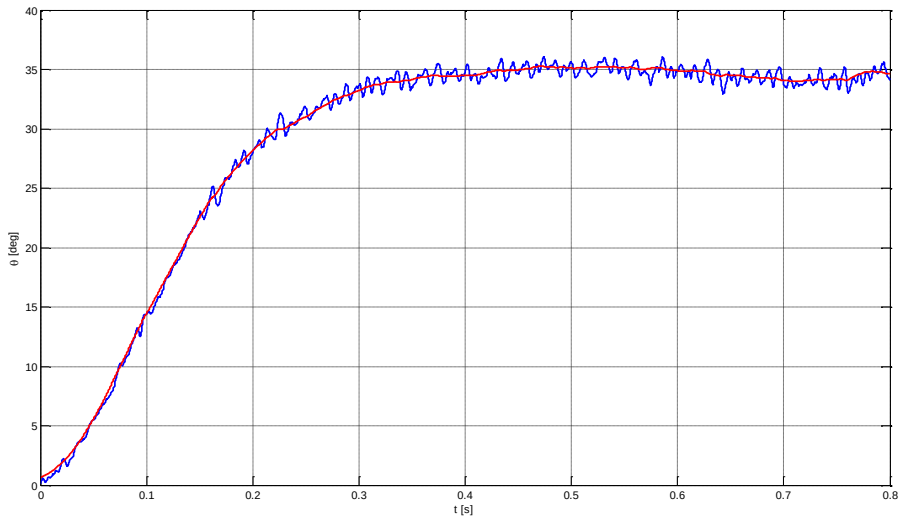

Figure 37: sensorless position control operation. Estimated stimated and measured angle with a step position reference equal to 35 deg., Vhf=150 V, ωhf=166 Hz

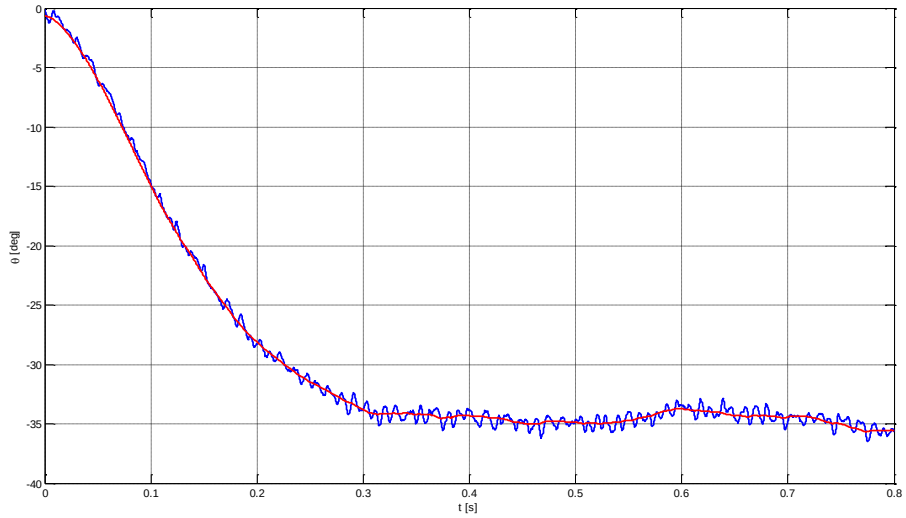

Figure 38: sensorless position control operation. Estimated stimated and measured angle with a step position reference equal to -35 deg., Vhf=150 V, ωhf=166 Hz

Reference position amplitude equal to 50 deg.

Fig. 39 and 40 show the waveform of the position control with a very low reference angle, in this case equal to 50 deg. with respectively a positive and negative reference sign, with an initial position equal to 0 deg. The rise time is 0,4 s and there are not overshoots.

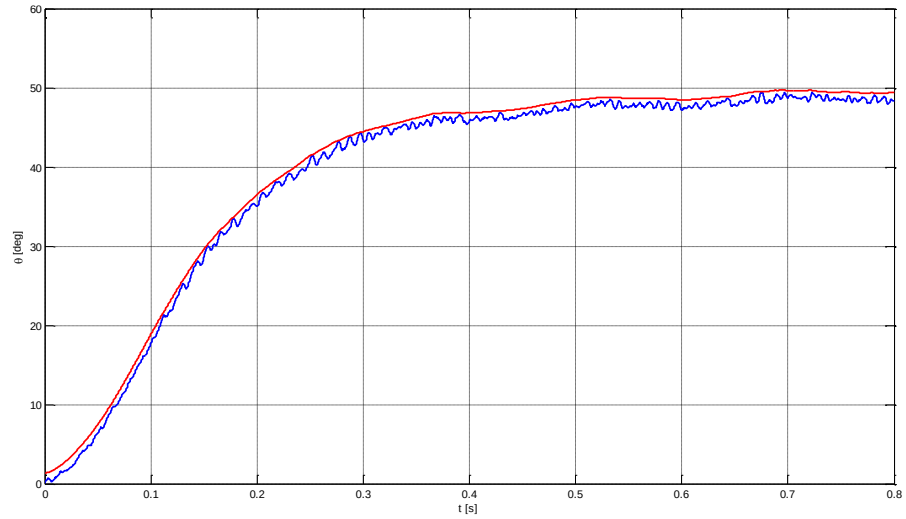

Figure 39: sensorless position control operation. Estimated stimated and measured angle with a step position reference equal to 50 deg., Vhf=150 V, ωhf=166 Hz

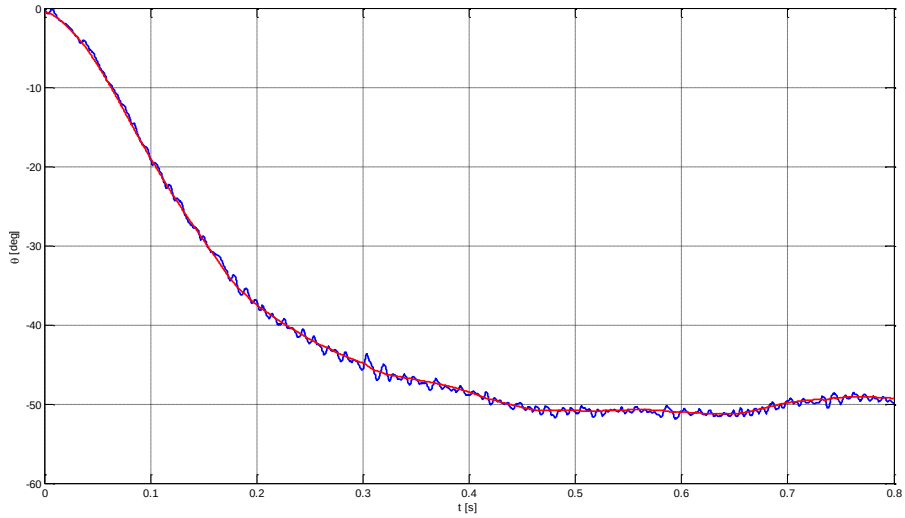

Figure 40: sensorless position control operation. Estimated and measured angle with a step position reference equal to -50 deg. , Vhf=150 V, ωhf=166 Hz

Reference position amplitude equal to 75 deg.

Fig. 41 and 42 show the waveform of the position control with a very low reference angle, in this case equal to 75 deg. with respectively a positive and negative reference sign, with an initial position equal to 0 deg. The rise time is 0,35 s and there are not overshoots.

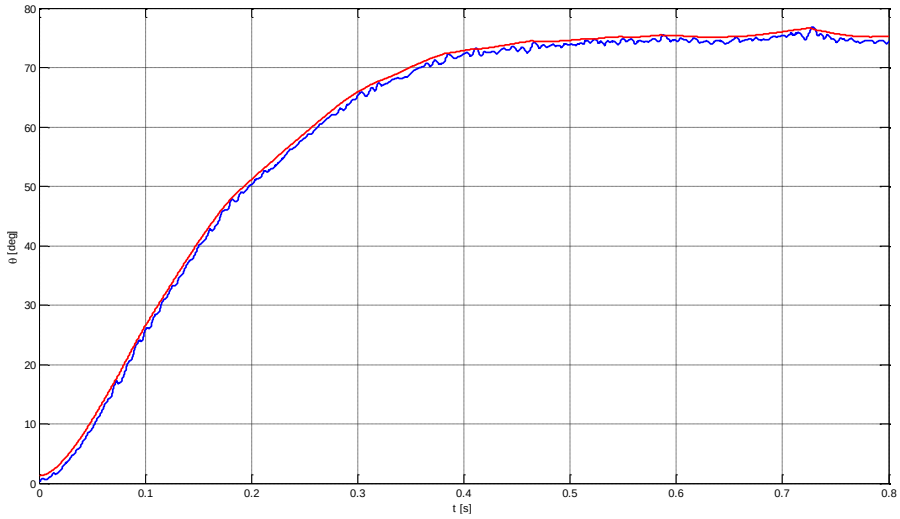

Figure 41: sensorless position control operation. Estimated stimated and measured angle with a step position reference equal to 75 deg., Vhf=150 V, ωhf=166 Hz

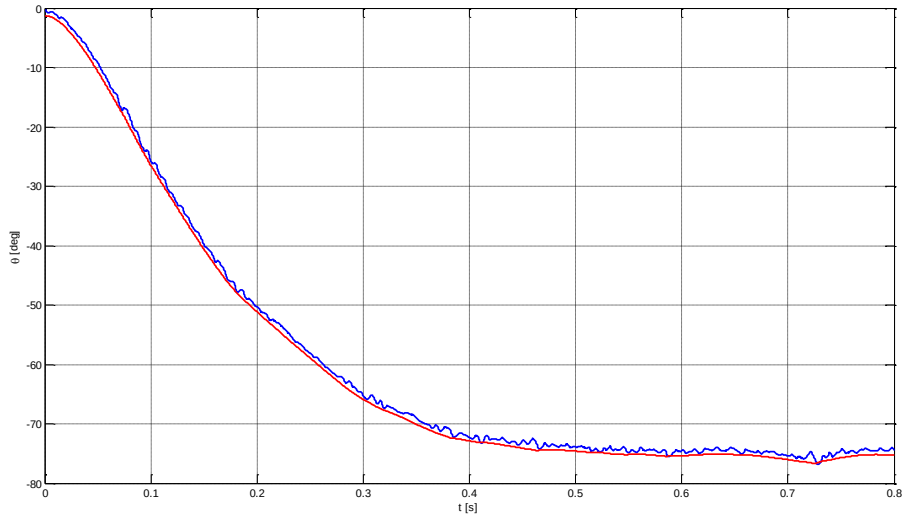

Figure 42: sensorless position control operation. Estimated stimated and measured angle with a step position reference equal to -75 deg., Vhf=150 V, ωhf=166 Hz.

Reference position amplitude equal to 90 deg.

Fig. 43 and 44 show the waveform of the position control with a very low reference angle, in this case equal to 90 deg. with respectively a positive and negative reference sign, with an initial position equal to 0 deg. The rise time is 0,4 s and there are not overshoots.

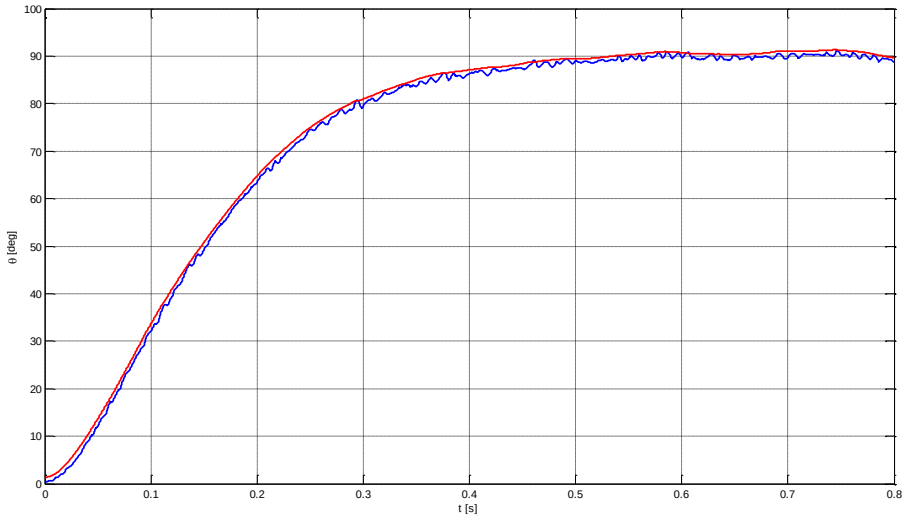

Figure 43: sensorless position control operation. Estimated stimated and measured angle with a step position reference equal to 90 deg., Vhf=150 V, ωhf=166 Hz

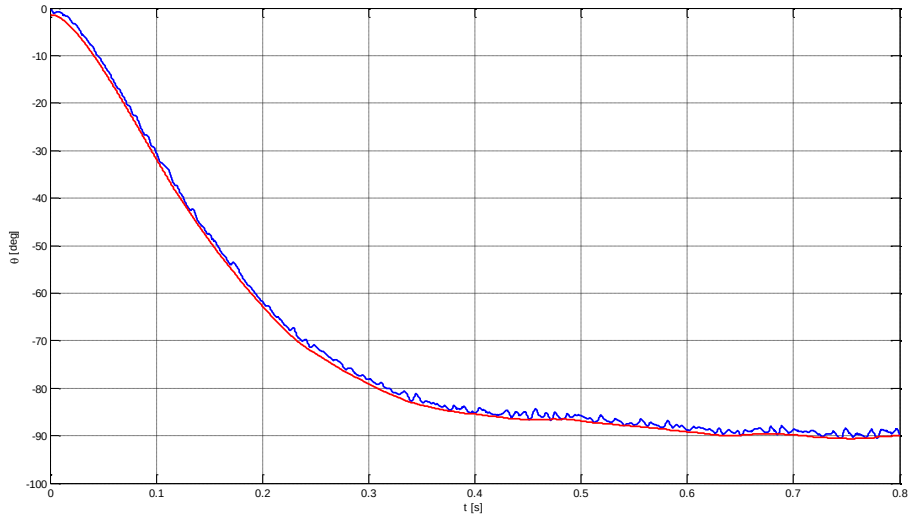

Figure 44: sensorless position control operation. Estimated stimated and measured angle with a step position reference equal to -90 deg., Vhf=150 V, ωhf=166 Hz

These were the last simulations about the control by HF technique. The obtained results are excellent, the control works always properly.

4 . Model reference adaptive system

This chapter is made of two main parts, the first explains the theory of the MRAS method used to control the RSM for medium and high speed, the second shows the results of the simulations, executed with Simulink and Matlab 2014a.

4.1 MRAS theory

The MBMSTs (model based method sensorless techniques) are used to control the electrical machine at medium and high speed. This methods use the electrical machine equation to estimate speed and position of the rotor using the back-EMF (electromotive force) induced in the stator wirings. To realize this control, it is necessary to know the values of the voltages and of the currents. The currents values are measured with a current transducers and the voltages values are obtained with PWM input signals. There are various types of MBMSTs, for example: open loop estimator, MRAS (model reference adaptive system) with close loop and closed loop observers.

The chosen method is the MRAS. A general structure is shown in Fig. 45.

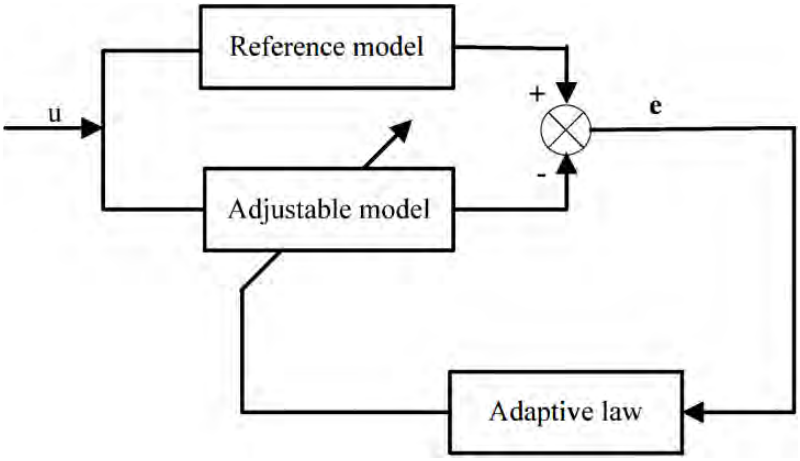

Figure 45: block diagram of the MRAS method

The Model Reference Adaptive System is a method to estimate speed and position of the rotor. This method uses two models, the first, called adaptive model, is equations containing the parameters of the machine and the speed, its output is the current expressed in the rotating reference frame. The second is the reference model, which expresses current and it doesn't depend on the speed. In this case, the output of the reference model is obtained measuring directly the a, b and c currents thanks to the transducers and the Prank transformations.

The MRAS method is applied only to high speeds, because it needs high amplitude of the electromotive force which is proportional to the rotor speed. To develop this control, it is necessary to make a model of the RSM. For the initial study, the magnetic circuit is considered linear and the PWM is bethought ideal.

- **Adjustable model**

Usually, in PMSMs, the MRAS estimator uses the flux of the permanent magnets to find the d axis, but a RSM has not PMs. For this motivation, the used signals to estimate the spatial information are the d and q currents. Using the voltage equations of the RSM in the rotating reference frame, described in the chapter 2, it is possible to get the derivatives of the d and q currents:

$$\frac{di_d}{dt} = v_d - Ri_d + \omega_e L_q i_q$$
$$\frac{di_q}{dt} = v_q - Ri_q - \omega_e L_d i_d$$

These equations are used to realise the adjustable model and its outputs are the d and q currents, thanks to two integrators.

Fig. 46 represents the adjustable model:

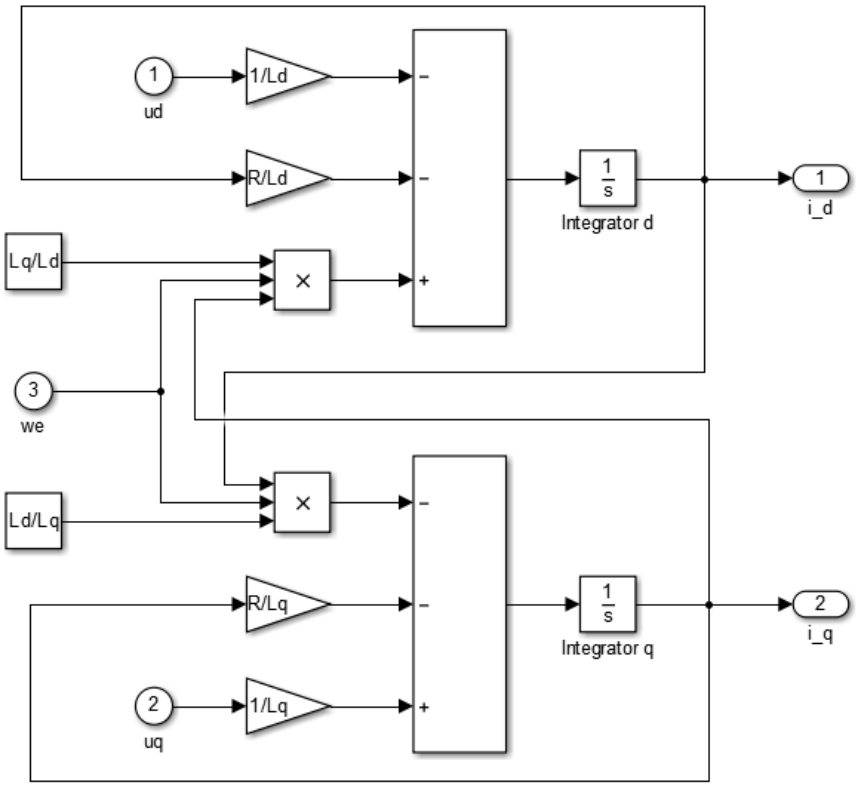

Figure 46: adjustable model

- **Reference model**

The reference model is given by the RSM and the current transducers and the measured d and q currents are the outputs of this model, like shown in Fig. 47.

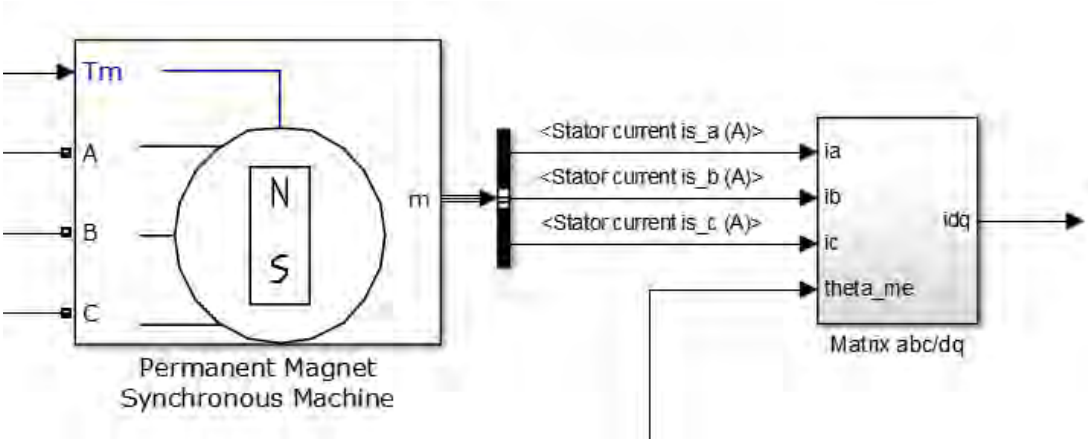

Figure 47: reference model

- **Adaptive law**

Now, it is necessary to obtain an information about the rotor speed and position. Since the two models should give the same output, with the same amplitude and phase, the idea for the control is to watch if the phases of the two models outputs are the same. This is realised with a vector product of the measured current vector with the estimated current vector and the result is divided with a squared cross amplitude, the final result is the error:

$$e_{MRAS} = \frac{i_{dq}^{*} \times \hat{i_{dq}}}{\left|i_{dq}^{*,\hat{}}\right|^2} = \frac{i_d^{*}\hat{i_q} - i_q^{*}\hat{i_d}}{i_d^{*}\hat{i_d} + i_q^{*}\hat{i_q}}$$

Afterwards, the error is sent to a PI regulator and the output is the estimated electric speed.

$$\omega_{MRAS} = K_P e_{MRAS} + \frac{K_I e_{MRAS}}{s}$$

Subsequently, the estimated rotor position is obtained with the integration of the estimated electric speed.

$$\theta_{MRAS} = \frac{\omega_{MRAS}}{s}$$

The structure of the adaptive law is displayed in Fig. 48.

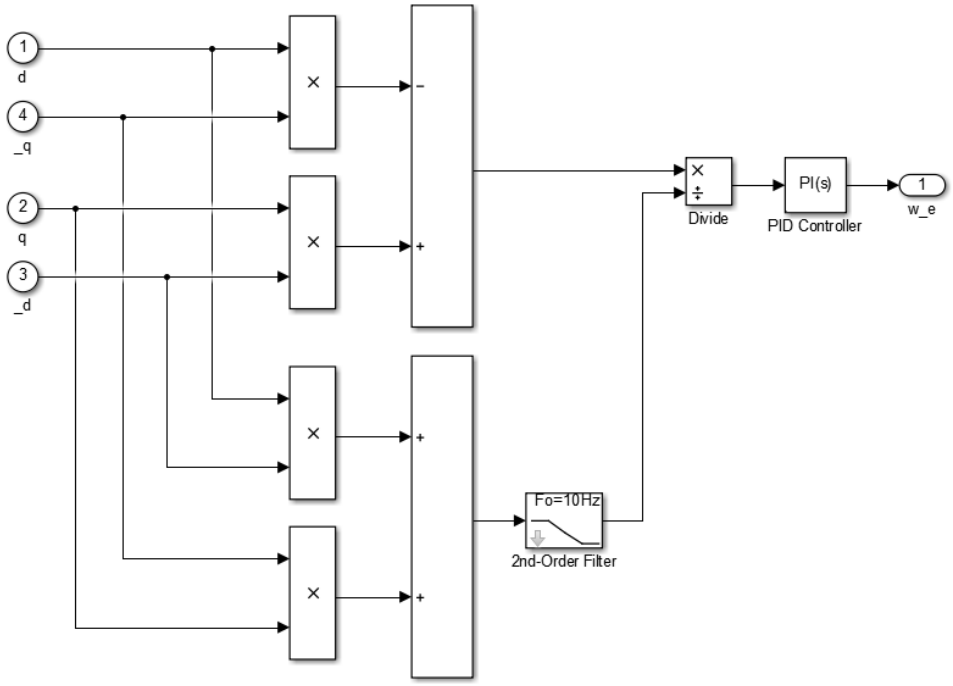

Figure 48: adaptive law

Now, the estimated electric speed is used to adjust the adjustable model, making a close loop, the MRAS structured is shown in Fig. 49.

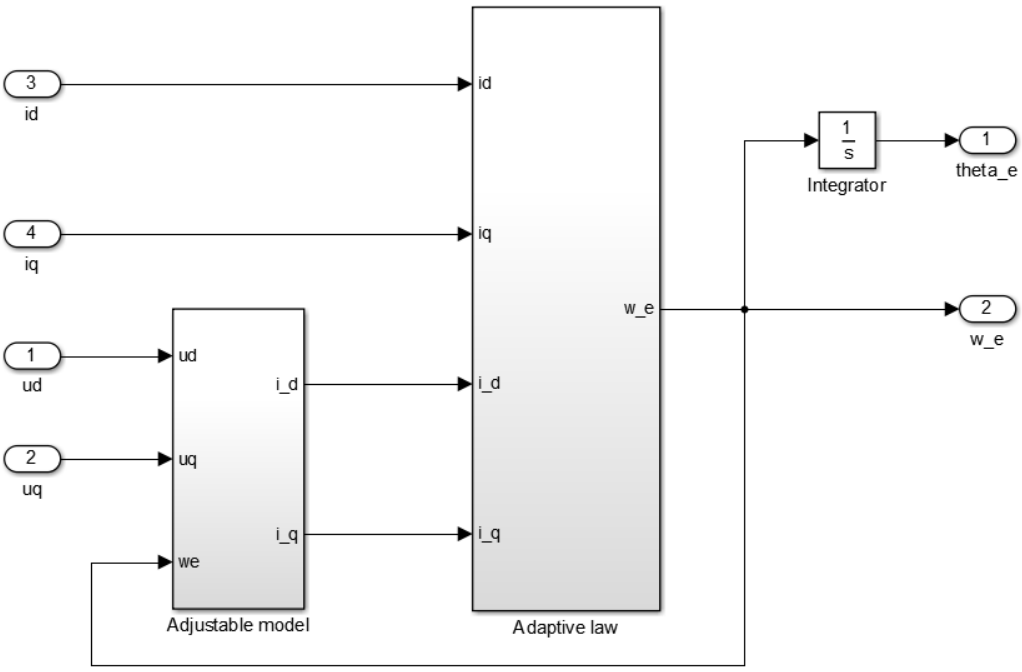

Figure 49: MRAS model

An equation to choose the values of the proportional and integral gains does not exist. The only method is to look at the different wave forms of all the models signals and to try to find the right values.

In this case, they result:

$$K_{P\,MRAS} = 9$$

$$K_{I\,MRAS} = 405$$

4.2 Simulations of the MRAS method

The simulation shows if the system is working properly and its performance. The MRAS method must control the RSM working at medium and high speeds and this part of the chapter contains the respective graphs. For the control it is necessary to know the initial position of the rotor, this information is obtained thanks to the high frequency method, how reported in the Chapter 2.

In the following paragraphs the different tests of the control al separately described showing the results.

4.2.1 Estimation of the rotor speed

The first step is to check if the speed value, estimated by MRAS blocks, is right. To do this in the simulation, the RSM is controlled by a current sensored control and its speed is imposed by an external reference. The MRAS method musts work with medium and high speed, so in the following graph it is shown the estimated speed in steady state at different speeds from 100 rad/s until 300 rad/s with a step of 50 rad/s. This part is necessary to set the proportional and integral coefficients of the PI regulator for the estimation of the speed by MRAS method.

Fig. 50 shows the measured and estimated speeds of the rotor with the MRAS method.

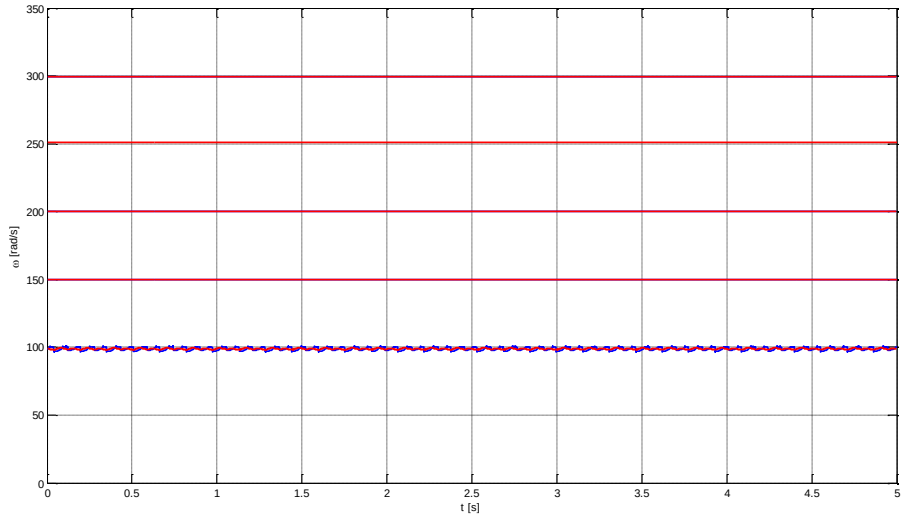

Figure 50: estimated (blue) and measured speed (red), for speeds 100, 150, 200, 250 and 300 rad/s

How it is shown in the graph, the program properly estimates the speeds, there is a little noise at the lowest speed that depends on the proportional coefficient of the PI regulators of the MRAS block. They are proportional, so if the proportional coefficient decreases, also the noise decreases but the performance of the estimation decrease during the transient state.

4.2.2 Current sensorless control

The second step is trying to use the current sensorless control. Remembering that the nominal current is equal to 3,9 A, the reference current is a step with a initial value equal to zero and a final value equal to the nominal current.

It is important that the current control has a great performance, or the speed sensorless control works improperly. In this part the method is tested to see if it can works with a primary sensorless control and how the system works with a current transient state. This is reported in Fig. 51.

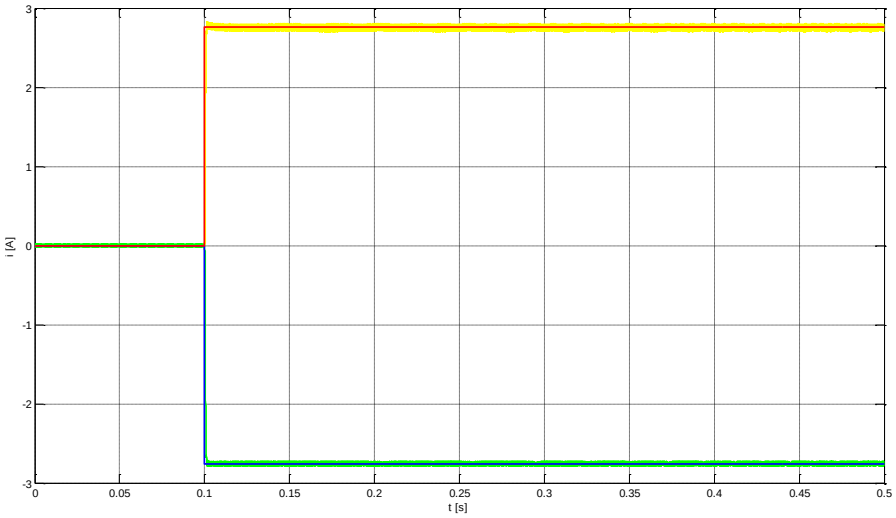

Figure 51: sensorless current control operation. Estimated d (blue) and q (red) currents with a current sensorless control

The Fig. 51 shows the performance of the current sensorless control, it is very fast, with a rise time about 0,05 s, it is stable and it has a neglecting overshot. The estimated d and q currents have the identical waveforms.

Fig. 52 displays theerror from the measured and estimated angle of the rotor.

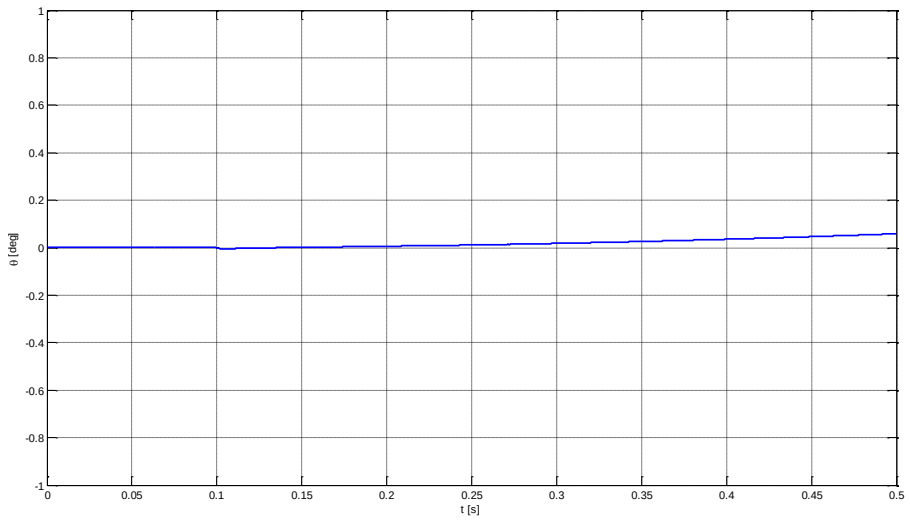

Figure 52: sensorless current control operation. Error angle during the current sensorless conrol

4.2.3 Speed senseless control

The last step is the speed sensorless control. It musts work in a speed range of ±100 rad/s until ±300 rad/s. So, successively the speed sensorless control performances are studied at these speeds and the graphs are reported in the following paragraphs.

Speed reference equal to 100 rad/s

Fig. 53 shows the estimated speed and the measured speed of the rotor. How it is possible to see, the rise time is about 0,5 s and there are not overshoots. This is the smallest reference speed amplitude that the sensorless control can follow. It the amplitude of the speed reference is lower the used signal to find the rotor speed is too small. In steady state, there is a little noise.

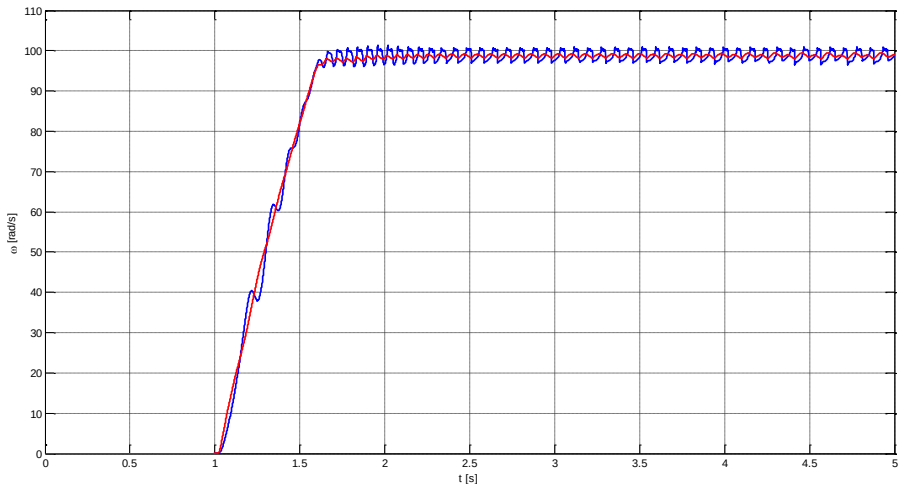

Figure 53: sensorless speed control operation. Estimated (blue) and measured (red) speed with a speed sensorless control realized with MRAS method with a speed reference equal to 100 rad/s

Fig. 54 shows the estimated rotor angle and the measured rotor angle. Observing the graphs, there is a little delay from the two signals in the first time of the simulation, due to the PLL because it needs a few time to find the right value. However during the transient, it decreases tending to zero.

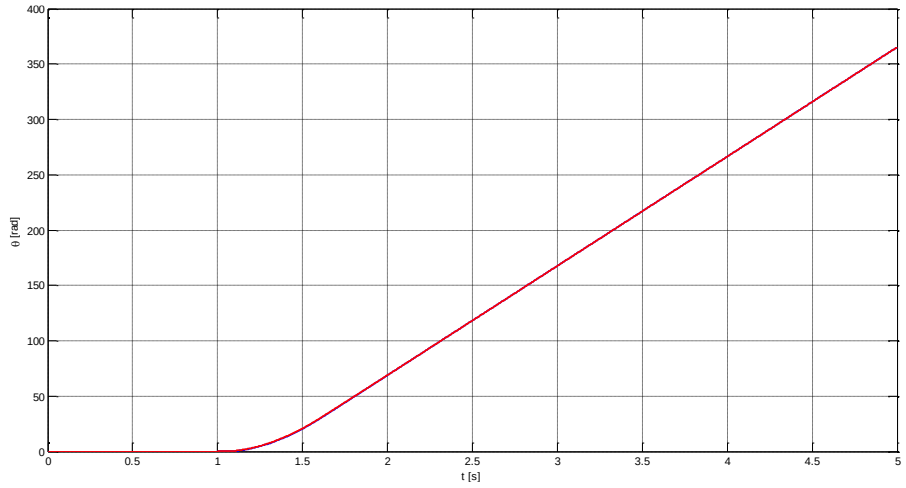

Figure 54: sensorless speed control operation. Estimated (blue) and measured (red) angles with a speed sensorless control realized with MRAS method with a speed reference equal to 100 rad/s

Speed reference equal to -100 rad/s

Fig. 55 shows the estimated speed and the measured speed of the rotor with the smallest reference speed amplitude but with a negative sign. More or less the transient is the same of the previous case. The control works properly, with a rise time about 0,6 s, it stable and a little noise is always superimposed to the estimated speed in steady state.

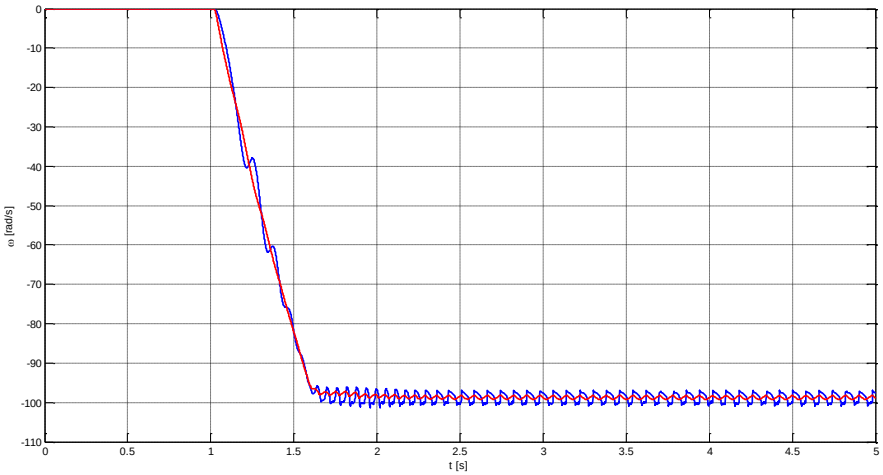

Figure 55: sensorless speed control operation. Estimated (blue) and measured (red) speed with a speed sensorless control realized with MRAS method with a speed reference equal to -100 rad/s

Fig. 56 shows the estimated rotor angle and the measured rotor angle. The obtained deductions, observing the graph, are the same of the antecedent case.

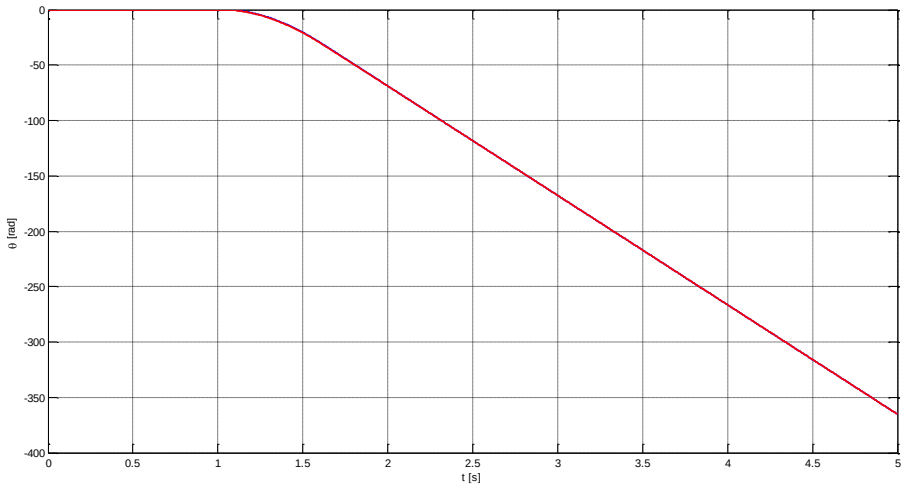

Figure 56: sensorless speed control operation. Estimated (blue) and measured (red) angles with a speed sensorless control realized with MRAS method with a speed reference equal to -100 rad/s

Speed reference equal to 300 rad/s

Fig. 57 shows the estimated speed and the measured speed of the rotor with the largest reference speed amplitude, due to the mechanical limit of the RSM. Also with this reference, the control works properly and it is stable, but in this case the rise time is higher, it is 2 s. There are not overshoots and the noise is lower, it decreases with increasing speed.

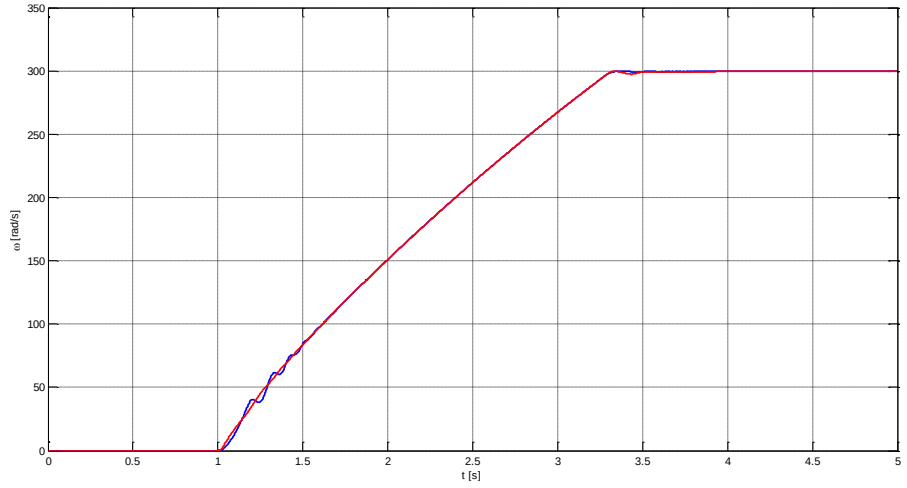

Figure 57: sensorless speed control operation. Estimated (blue) and measured (red) speed with a speed sensorless control realized with MRAS method with a speed reference equal to 300 rad/s

Fig. 58 shows the estimated rotor angle and the measured rotor angle. Also with this reference there are not problems with the estimation of the angle.

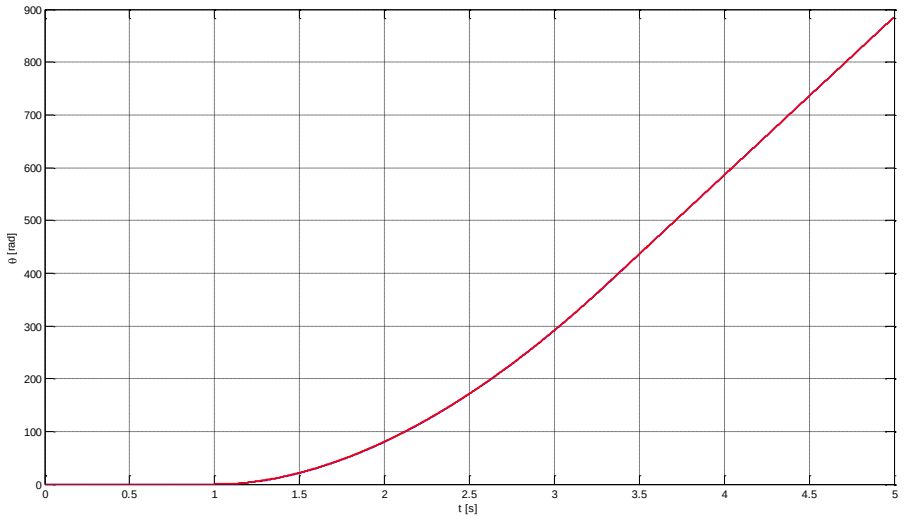

Figure 58: sensorless speed control operation. Estimated (blue) and measured (red) angles with a speed sensorless control realized with MRAS method with a speed reference equal to 300 rad/s

Speed reference equal to -300 rad/s

The Fig. 59 shows the estimated speed and the measured speed of the rotor with the bigger reference speed amplitude but with a negative sign. The obtained waveform of the estimated speed has the same characteristics of the estimated speed waveform with a reference speed equal to -300 rad/s.

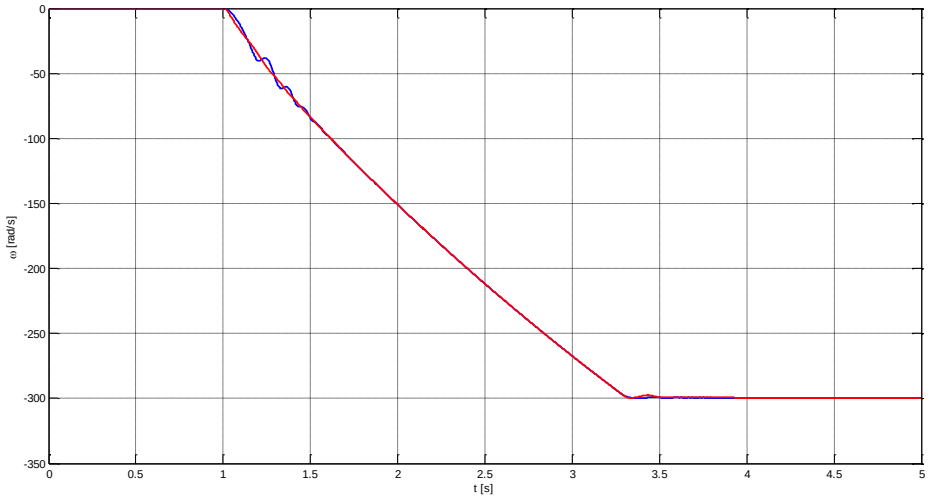

Figure 59: sensorless speed control operation. Estimated (blue) and measured (red) speed with a speed sensorless control realized with MRAS method with a speed reference equal to -300 rad/s

Fig. 60 shows the estimated rotor angle and the measured rotor angle.

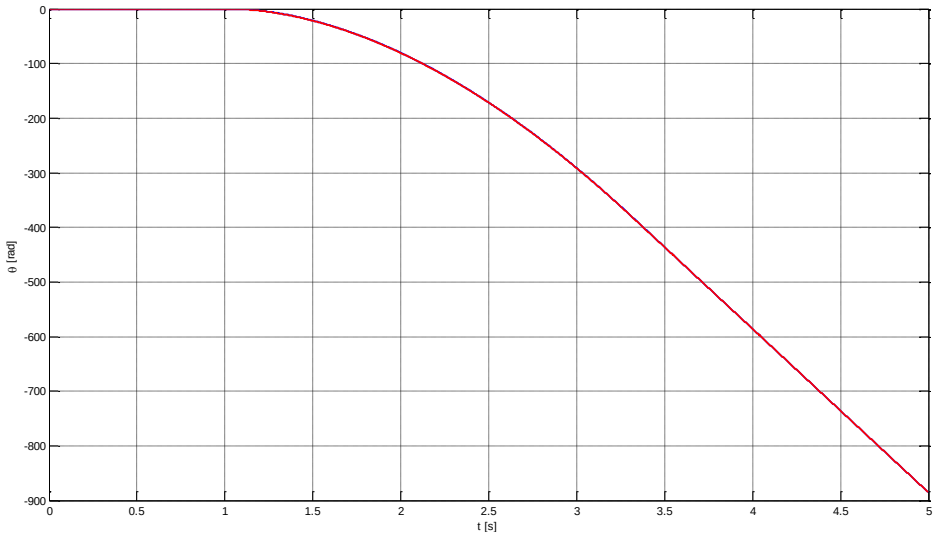

Figure 60: sensorless speed control operation. Estimated (blue) and measured (red) angles with a speed sensorless control realized with MRAS method with a speed reference equal to -300 rad/s

5 . Experimental results

5.1 Introduction

This Chapter shows the obtained results with the HF and MRAS methods for the sensorless control. First it showed the HF technique and after the MRAS technique. To develop all the control, it is used the software CCS (code composer studio), realized by TI (Texas Instrument). This software is an IDE (integrated development environment), which can support only TI microcontroller. The used language for the programming is close to C/C++.

Simulink works with the Laplace transformation, but CCS no, it works with the Z transformation. It is necessary to convert the transfer function from Laplace transformation in Z transformation.

Fig. 61 shows the structure of the test bench.

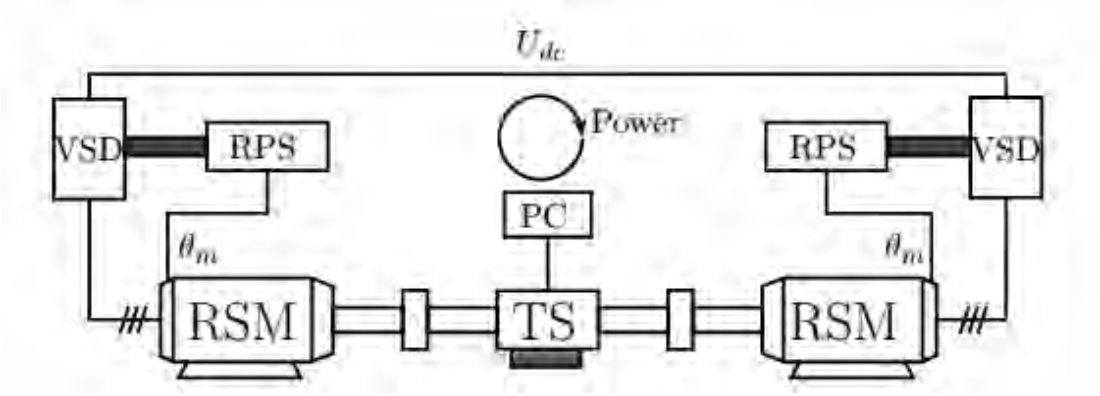

Figure 61: electric scheme of the test bench

The test bench is composed with:

- RSM: it is used with the different sensorless controls, it has also an encoder to measure the rotor speed and rotor position.

- IM: it is controlled with a sensored control with a very high accuracy, this machine is used like load for the RSM and also to test the estimation speed

and position with the sensorless methods. The RSM and IM shafts are connected thanks a coupling.

- IM AC/AC: this convertor is necessary to control the IM and it takes the electrical energy from a three-phase line.

- RSM AC/AC: this is converter that supplies the RSM. Basically it takes the electrical energy from a three-phase line, the voltage is rectified with an AC/DC converter made by three boughs, everyone is made by two non-controlled diodes and every phase line is connected in one bough, between the two diodes. The AC/DC converter output is connected with a capacitor in parallel with a HPF, capacitor keeps a constant voltage and HPF do not allow at the noises to enter in the inverter control, the constant voltage is measured and if it has a too high value, the power source will be interrupted. At the final, this voltage supplies a DC/AC convert, which is controlled by six IGBT transistors. The outputs of the CD/AC converter supply the RSM.

- Computer: the programs to control RSM and IM are executed by the computer. It is shown in Fig. 62.

Figure 62: test bench

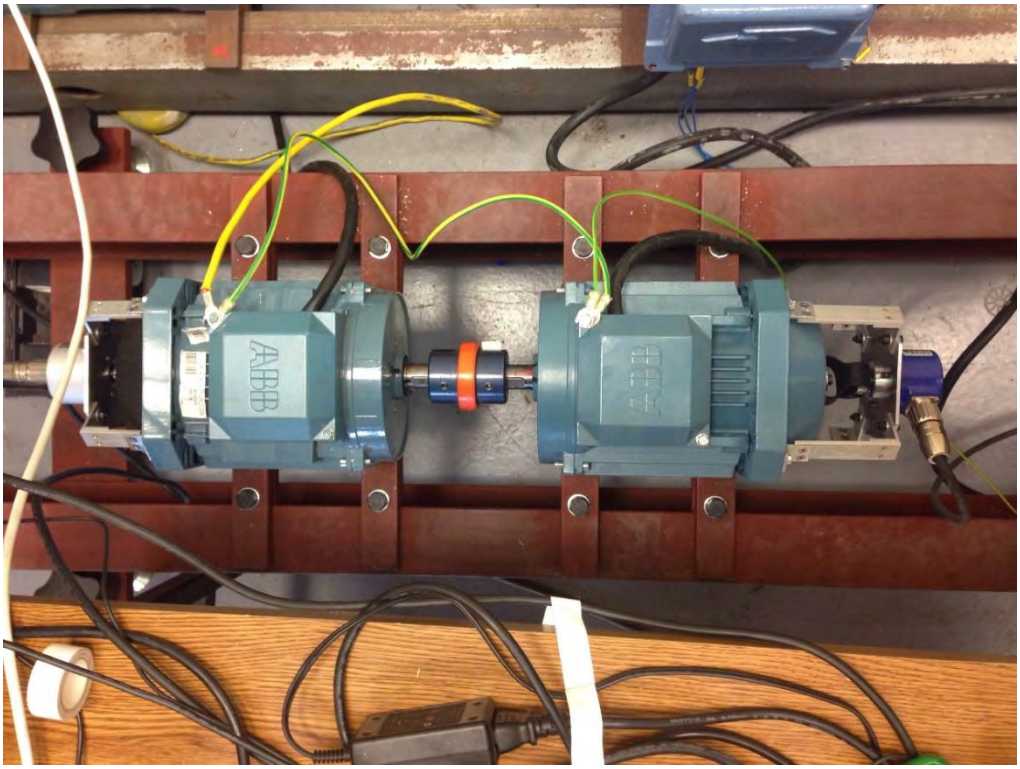

Figure 63: RSM and IM with the coupled shafts

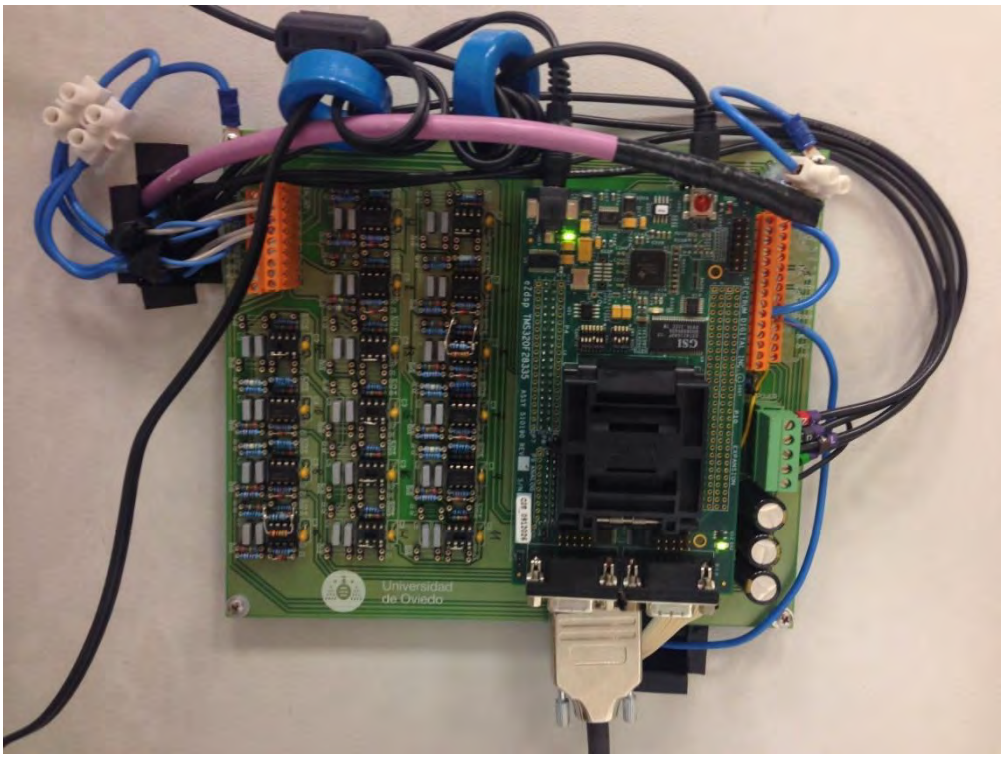

Figure 64: DSP breadboard

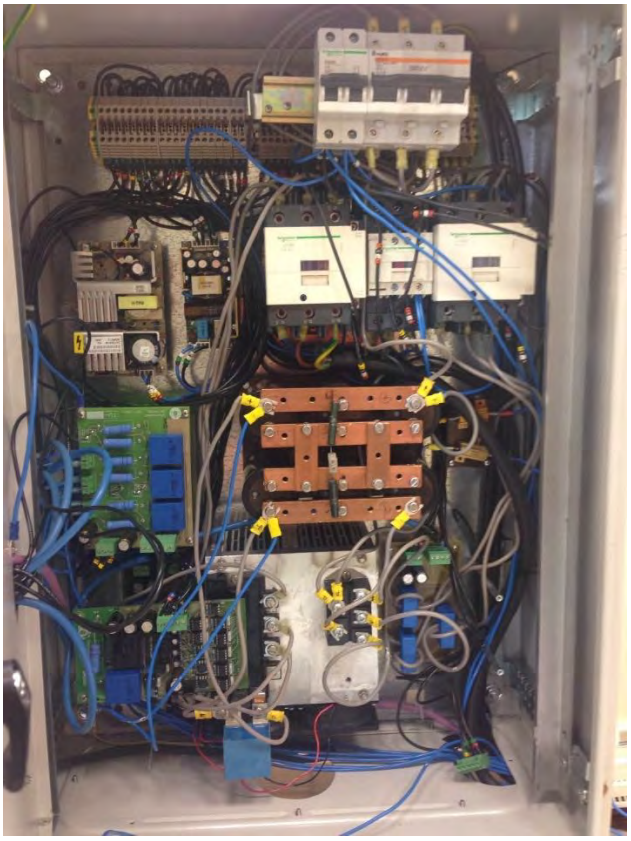

Figure 65: AC/AC converter

5.2 High frequency method

The practical implementation of the HF method to realize a position and low speed control is completed. The programs are written with CCS. The programs have the same structure of the developed programs in Simulink, more or less. Simulink works in an ideal world, so it cannot considered the problems that it is possible to find in a real case. Therefore, the program has been changed a little bit to can work properly.

The main problems are:

- Saturation of the machine
- Dead-time of the inverter
- PWM strategy
- Accuracy of the currant Hall sensors.

The heaviest prblem is the resolution of the current Hall sensors, because the used transtucers is a LA 50-P, ita can measure DC, AC and pulsed curent, and it makes a galvanic isoltion between the primary circuit (high power) and the secondary circuit(electronic power). However, its nominal current is 50 A and the HF current, used to find the spatial information has an amplitude of 0,55 A, with a voltage of 150 V and a frequency of 166 Hz of the injected HF voltage signal. Value of the HF current amplitude, is the motivation of the values of the voltage and frequency chosen. The d and q high frequency currents must have a sinusoidal waveform. Initially, the noise had a too high amplidute, so it hab been necessary to change some resistances of the ciruciut for the measure of the currents. This circuit is made by two OA (operational amplifier), like shown in Fig. 66, where the first OA is used like voltage divider and the second OA is used to measure the output of the first OA, its output is sent to the DSP. Following, with the calculated filters on Simulink, the program didn't work properly, the new their values are chosen with different experimental attempts.

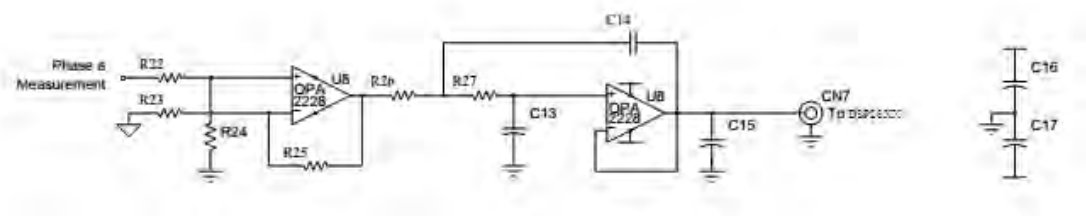

Figure 66: electronic scheme to measure a phase current

Thanks to the encoder, a strong speed control has been created

5.2.1 Estimation of the speed

The second step to develop the high frequency method is to estimate the electric speed. To test this part of the program, the IM was controlled with a speed sensored control and only the HF signal was injected in the RSM. At the different of the estimated angle which is obtained with the integration of the electric speed, the estimated speed has a noise and its amplitude increases with the increment of the speed. It is necessary to seep the estimated speed with a LPF, so the estimation results right also at medium speeds. Anyway, the filter cannot have a too low cut-off frequency or it introduces a delay on the speed and this is a problem with the estimation of a step speed. The right value of the filter has been found only with experimental tests.

Fig. 67 displays the estimated speeds in steady state of the with different rotor speeds.

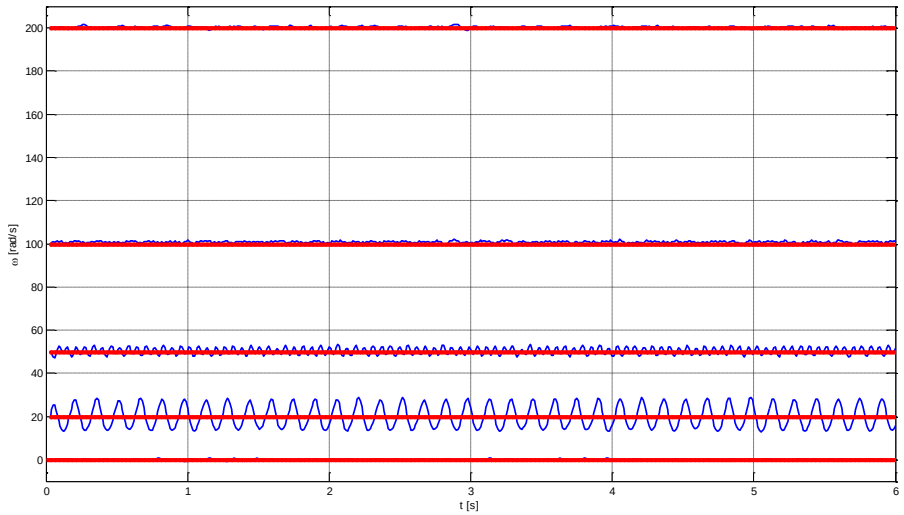

Figure 67: estimated (blue) and measured speed (red), for speeds 0, 20, 50, 100 and 200 rad/s. Vhf=150 V, ωhf=166 Hz, Iq=0, Id=0

Fig. 68 shows the estimated speed with a step speed.

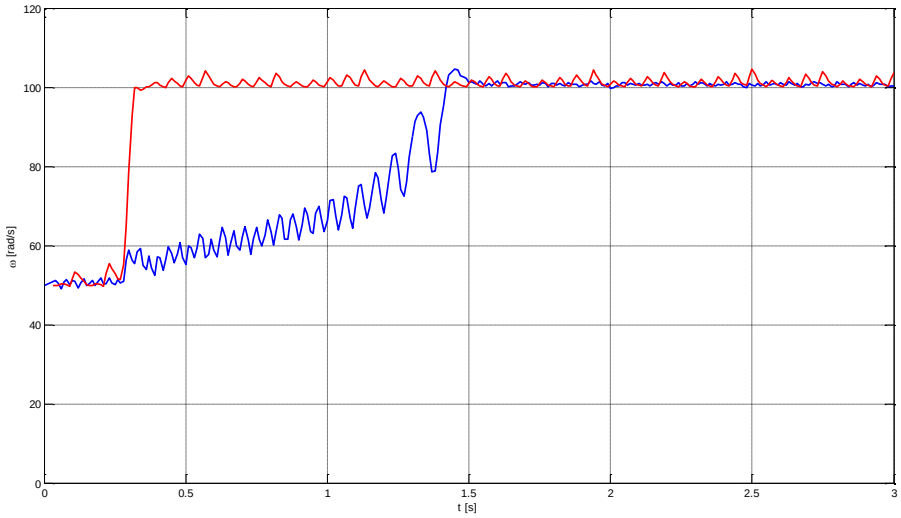

Figure 68: estimated (blue) and measured speed (red) during a speed transient. Vhf=150 V, ωhf=166 Hz, Iq=0, Id=0

5.2.2 Estimation of the angle

The way to develop this control is the same used in Simulink. The first step is to inject only the HF component in the RSM, without the fundamental component, trying to estimate the electric angle. To be sure of the correct estimation, before the RSM was supplied injecting a voltage signal with an amplitude about 40 V on the d axis in the stationary reference frame, so the RSM rotor is lined up with the real d axis. Successively, with the position control of the IM, the RSM rotor was locked. In this condition, the program for the estimation of the electric angle was tried. Fig. 69 shows the estimation of the angles with different position of the rotor.

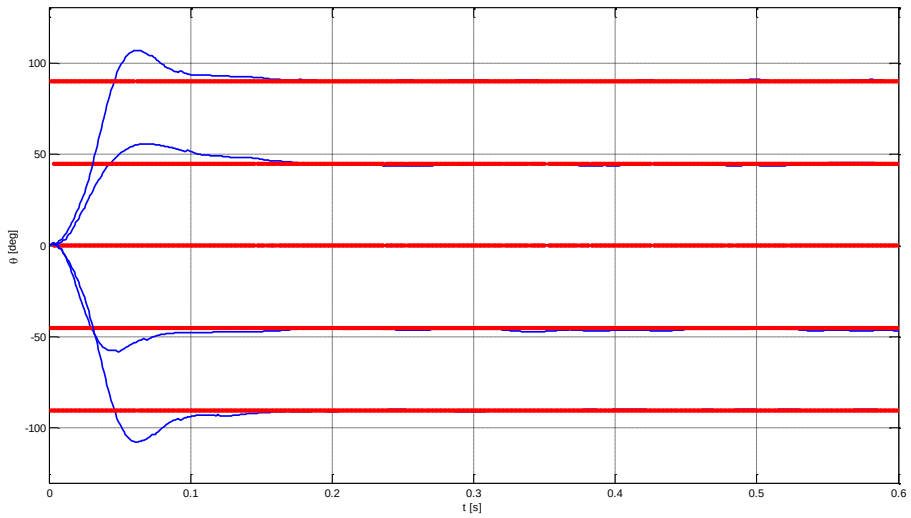

Figure 69: estimated (blue) and actual position (red), after the high frequency voltage is injected, for initial positions of -90, -45, 0, 45 and 90 deg. respectively. Vhf=150 V, ωhf=166 Hz, Iq=0, Id=0, ωr=0 Hz

5.2.3 Current control

Next step is to realize a current sensorless control thanks to the HF method. Only with a right current control it is possible to obtain a good speed sensorless control. This test is important to see if the filters work properly. In the transient state, part of the fundamental current could influence the estimated speed and position, causing a wrong control of the RMS. The current PI regulators were calculated with the equations of the Chapter 2. Before, it is important to test if the current regulators work properly. This is done injecting a reference step current in d axis and after in q axis with the rotor locked. Thanks to oscilloscope, the a and b currents are watched and the saved values by oscilloscope are elaborated with Matlab, finding the waveforms of d and q currents. The speed rotor is always controlled with the IM. In steady state, the programs works always right. It is important to control the effect of the saturation on the estimation of the angle. With the rotor at different speed values, giving a current step reference equal to the maximum value of the current, like shown in Fig. 70 it is observed that the current sensorless control works properly.

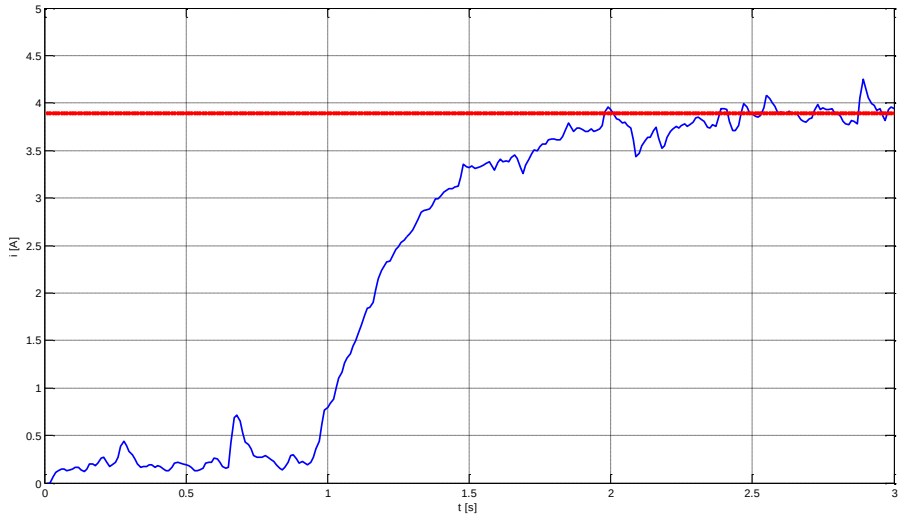

Figure 70: sensorless current control operation. Measured d (blue) and q (red) currents, estimated d (green) and q (yellow) currents. Vhf=150 V, ωhf=2*π*166 Hz, ωr=100 rad/s

In Fig. 71 it is shown the estimated and measured speed of the rotor. Wacthing it, it is possible to see that the system works properly.

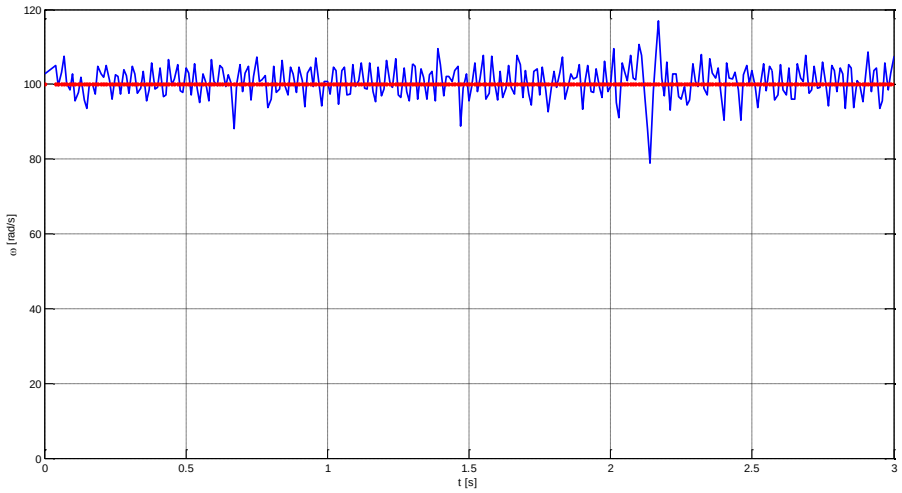

Figure 71: sensorless current control operation. Estimated (blue) and measured (red) speed of the rotor. Vhf=150 V, ωhf=2*π*166 Hz, ωr=100 rad/s

Fig. 72 shows the error angle introduced from the saturation of the machine. The error angle is very low, it is approximately equal to 2 deg., so it is deduced that the part of estimation works right.

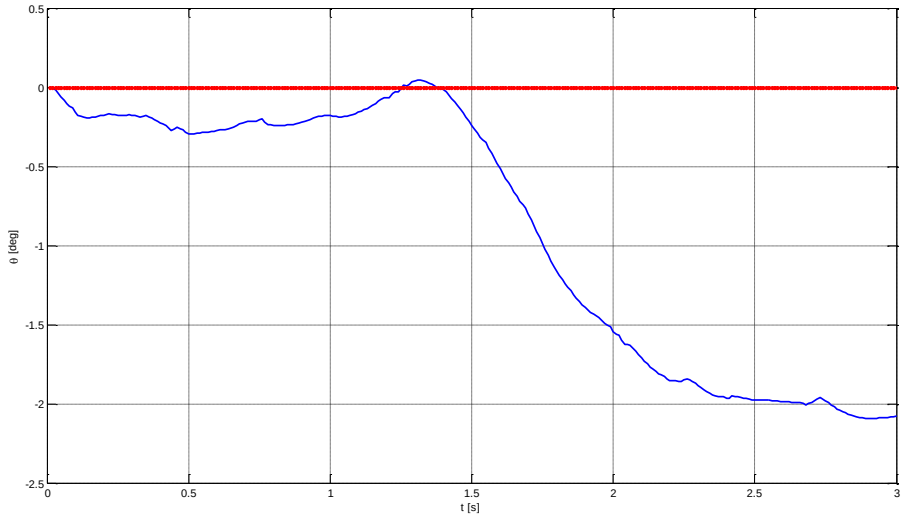

Figure 72: sensorless current control operation. Measured angle error (blue). Vhf=150 V, ωhf=2*π*166 Hz, ωr=100 rad/s

5.2.4 Speed control

Thanks to a right current sensorless control that works properly also with the maximum current, the next step is to develop a speed sensorless control. Typically, with a HF method it is possible to control a machine until the 30% of the maximum speed.

Fig. 73 shows the performance of the speed control, the rise time is very short and the control works right with every speed value in the range of -100 rad/s until 100 rad/s. In this range, the control can works properly also with a noise torque. It can works with a speed amplitude equal to 130 rad7s if there is not noise torque. With a reference speed higher than 130 rad/s the estimation of the rotor speed and position fails, due to the noises that acquire a too elevate amplitude, distorting the negative sequence. It is interesting to see how the estimated speed follows always the measured rotor speed by encoder, even though the overshoots.

The overshoots can be deleted choosing an integration coefficient of the speed PI regulator.

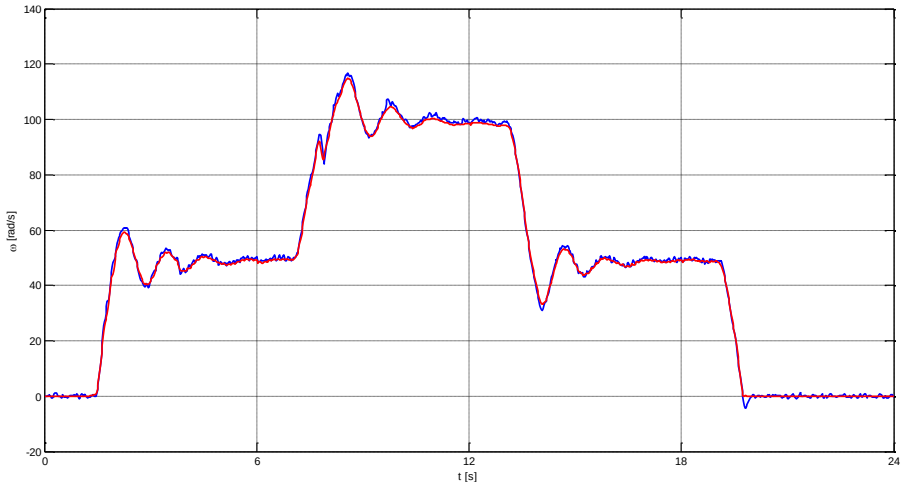

Figure 73: sensorless speed control operation. Measured (red) and estimated (blue) speed with different step speed reference. Vhf=150 V, ωhf=2*π*166 Hz

5.2.5 Position control

The last use of the HF technique is to make a position sensorless control.

With the coefficients values of the speed and PLL regulators it is not possible to obtain a position control. To obtain it, it is necessary a great very low speed sensorless control. For this motivation all the integration coefficients have been decrease and the proportional coefficient have increase. With these new values, in case of a speed control, the control can work only with a reference speed equal to the 10% of the maximum rotor speed.

In theory, the position regulator needs only a right proportional coefficient. However with the target to increase the rise time, the position regulator is a PI regulator. Its proportional coefficient is chosen like explained in the Chapter 2 and integration coefficient is chosen experimentally. The following graphs show the performance of the position control with different position references.

Reference angle amplitude equal to 35 deg.:

Fig. 74 and 75 show the waveform of the position control with a very low reference angle, in this case equal to 35 deg. with respectively a positive and negative reference sign, with an initial position equal to 0 deg.. In both the graphs, the rise time is large and there is a small overshoot, due to the position regulator integration part that sees a little error.

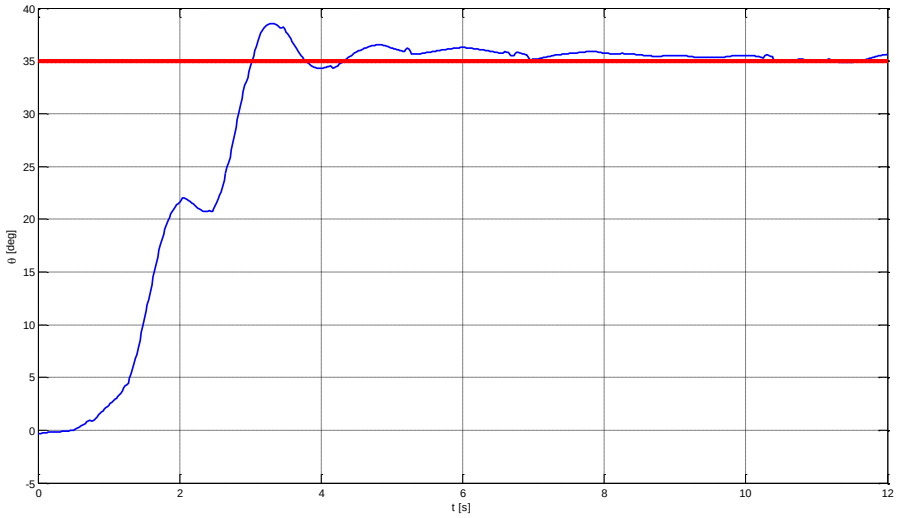

Figure 74: sensorless position control operation. estimated angle (blue) with a step position reference equal to 35 deg. (red) . Vhf=150 V, ωhf=2*π*166 Hz

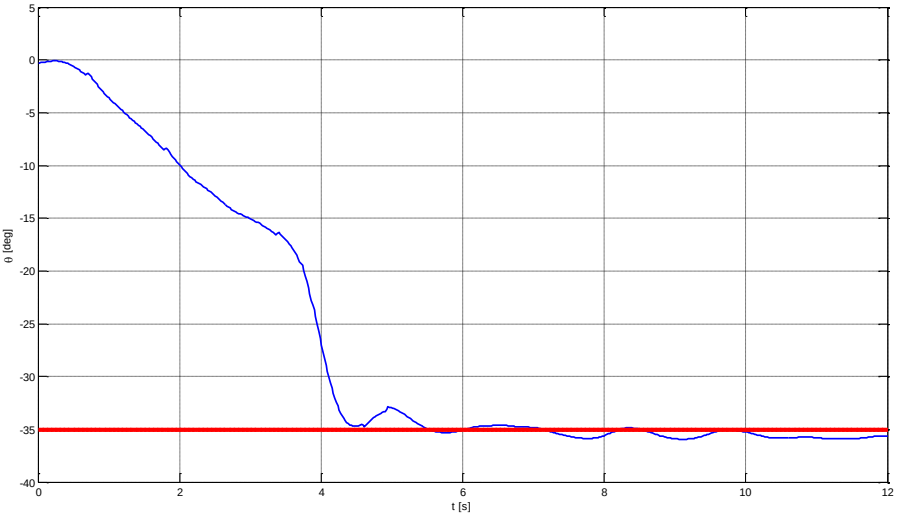

Figure 75: sensorless position control operation. Estimated angle (blue) with a step position reference equal to -35 deg. (red) . Vhf=150 V, ωhf=2*π*166 Hz

Reference angle amplitude equal to 50 deg.:

Fig. 76 and 77 show the waveform of the position control with a low reference angle, in this case equal to 50 deg., with respectively a positive and negative reference sign, with an initial position equal to 0 deg. In both the graphs, the rise time is shorter than previous cases and the overshoot is bigger, due to the position regulator integration effect.

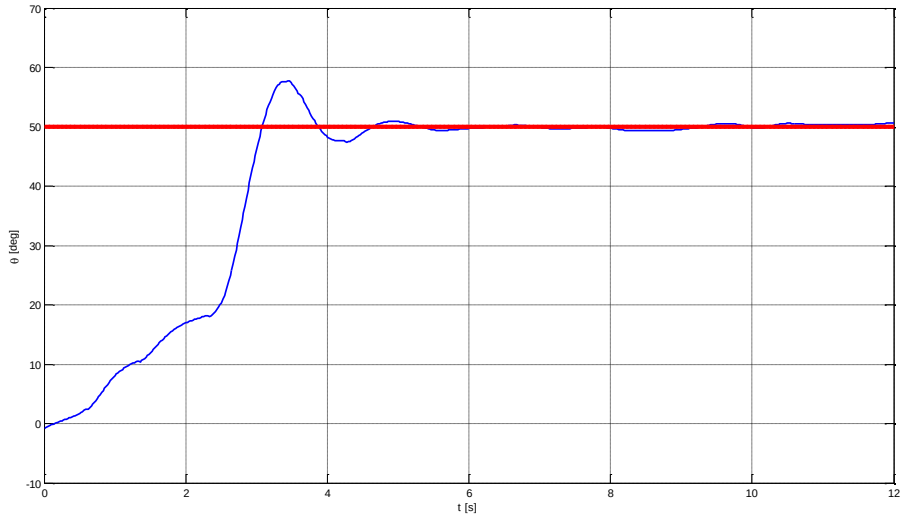

Figure 76: sensorless position control operation. Estimated angle (blue) with a step position reference equal to 50 deg. (red) . Vhf=150 V, ωhf=2*π*166 Hz

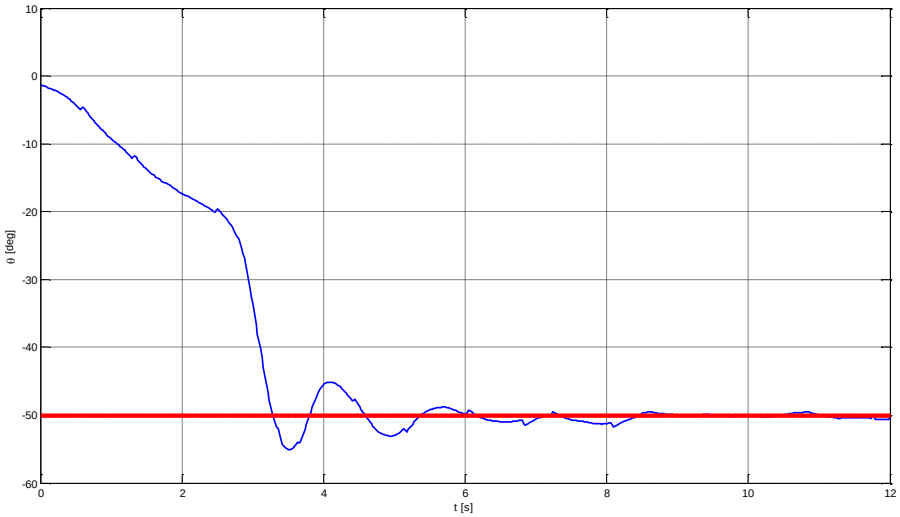

Figure 77: sensorless position control operation. Estimated angle (blue) with a step position reference equal to -50 deg. (red) . Vhf=150 V, ωhf=2*π*166 Hz

Reference angle amplitude equal to 75 deg.:

Fig. 78and 79 show the waveform of the position control with a low reference angle, in this case equal to 75 deg., with respectively a positive and negative reference sign,

with an initial position equal to 0 deg. Now the rise time is shorter than previous cases, thanks to the position regulator integration effect.

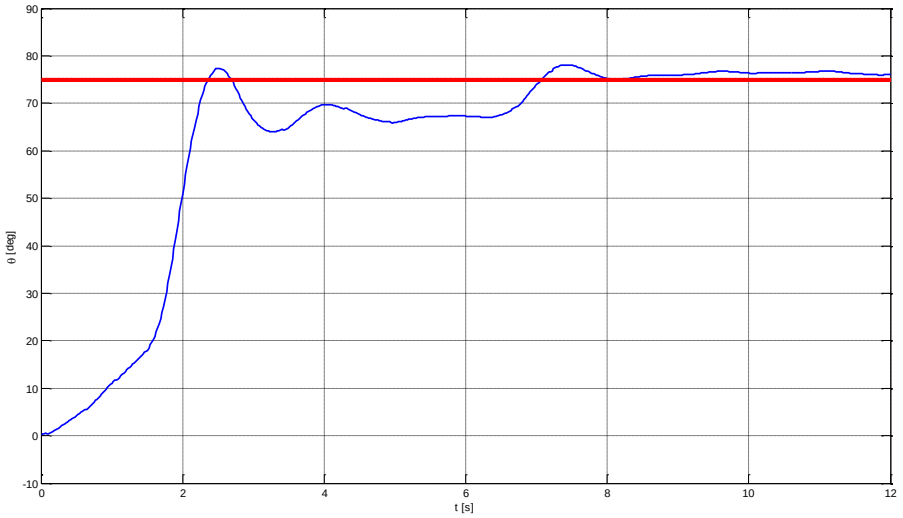

Figure 78: sensorless position control operation. Estimated angle (blue) with a step position reference equal to 75 deg. (red) . Vhf=150 V, ωhf=2*π*166 Hz

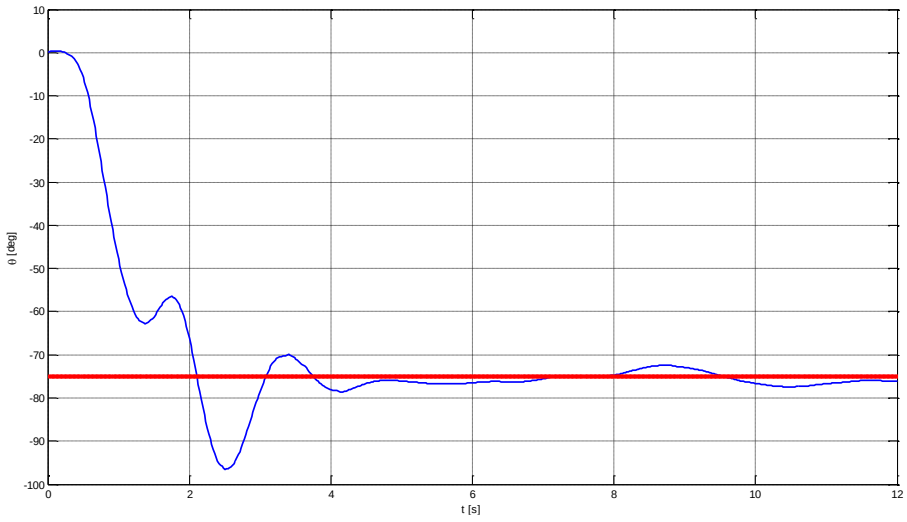

Figure 79: sensorless position control operation. Estimated angle (blue) with a step position reference equal to -75 deg. (red) . Vhf=150 V, ωhf=2*π*166 Hz

Reference angle amplitude equal to 90 deg.:

Fig. 90 and 91 show the waveform of the position control with a low reference angle, in this case equal to 90 deg., with respectively a positive and negative reference sign,

with an initial position equal to 0 deg. Now the rise time is shorter than previous cases, however the overshoots acquire a significant value, due to the position regulator integration effect. Anyway, whit a setting time equal to 8 s, the rotor reaches the wanted position.

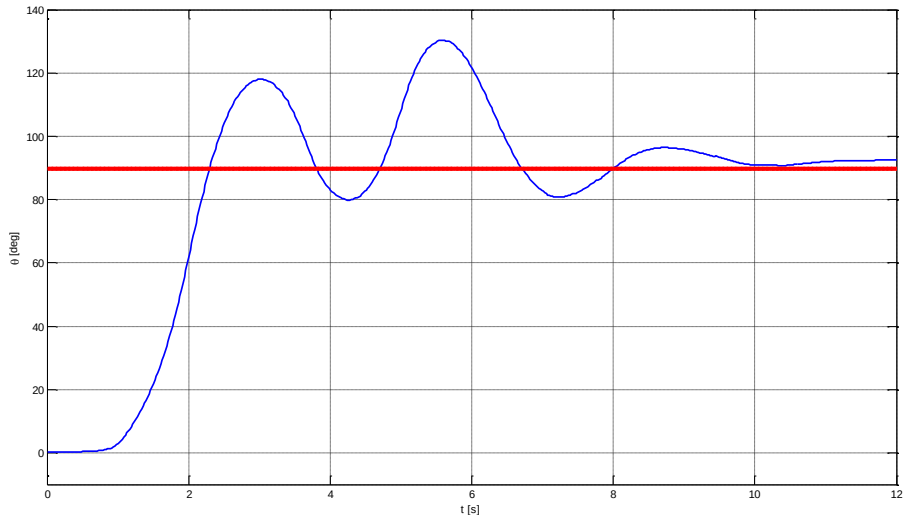

Figure 80: sensorless position control operation. Estimated angle (blue) with a step position reference equal to 90 deg. (red) . Vhf=150 V, ωhf=2*π*166 Hz

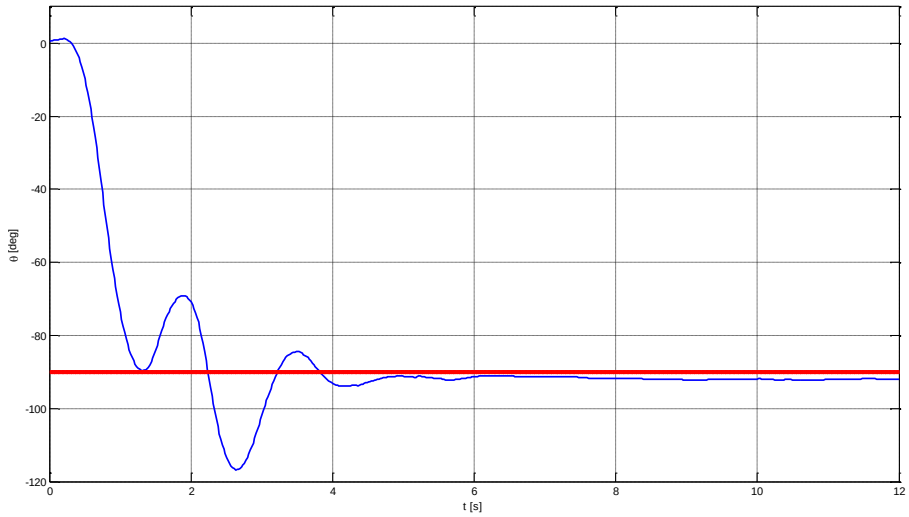

Figure 81: sensorless position control operation. Estimated angle (blue) with a step position reference equal to -90 deg. (red) . Vhf=150 V, ωhf=2*π*166 Hz

5.3 MRAS method

The Chapter 5 shows the theory about the MRAS method, how it is implemented in Simulink and the obtained results. It can appear easier to implement respect the HF method because the blocks numbers are lower.

The main program is composed by two main parts:

- First part: the MRAS method needs to know the initial position of the rotor, so it is used the HF program to estimate the electric position.

- Second part: after to know the initial position of the rotor, the program leave the HF method and it starts to use the MRAS method.

5.3.1 Estimation of the speed

Like executed in Simulink to develop the control, before it is necessary to test if the method estimates correctly the speed. To test this, IM keeps different constant speeds and a current control by sensor is used on the RSM with a current reference equal to 1 A. Fig. 82 shows the estimated speeds.

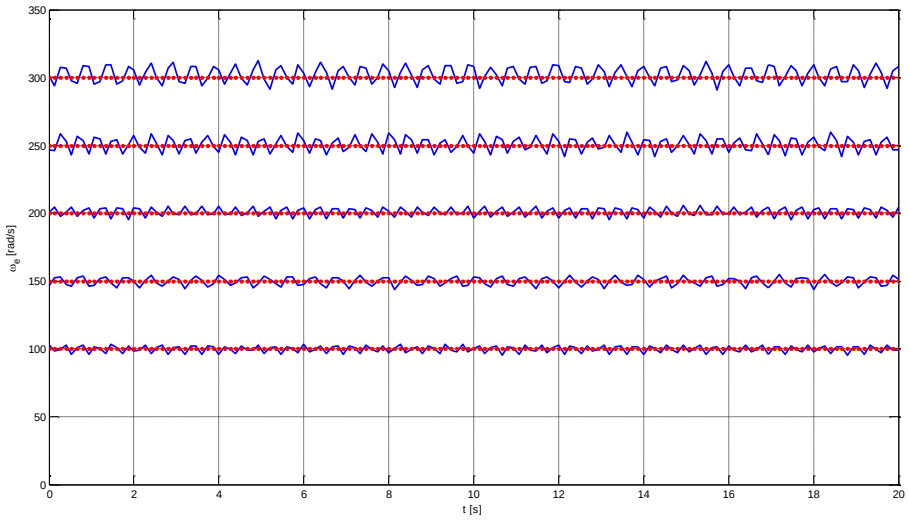

Figure 82: estimated (blue) and measured speed (red), for speeds 100, 150, 200, 250 and 300 rad/s

5.3.2 Current control

The next step is to test the current sensorless control. In this case, the non-ideal inverter and the heavy saturation of the RSM cannot a right control.

It is necessary to compensate them, how it is realized the two compensation is shown in appendix.

Figure 83 shows the waveform of the d and q estimated and measured currents with a step reference from 0 A to the nominal current.

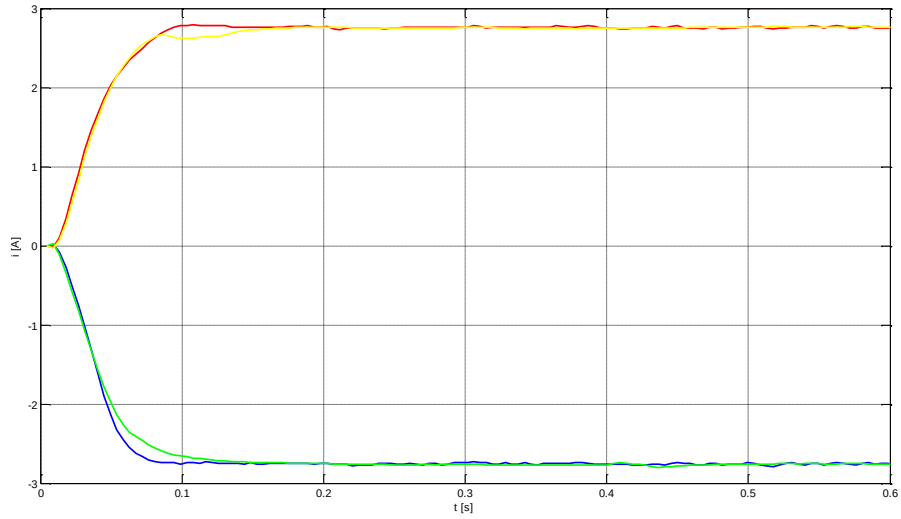

Figure 83: sensorless current control operation. Estmated d (green) and q (yellow) currents and measured d (blue) and q (red) currents with MRAS method with the compensation of the saturation

Also realized for the HF, it is observed the introduced error with the nominal current.

Fig. 84 displays the estimated angle error with a current step reference.

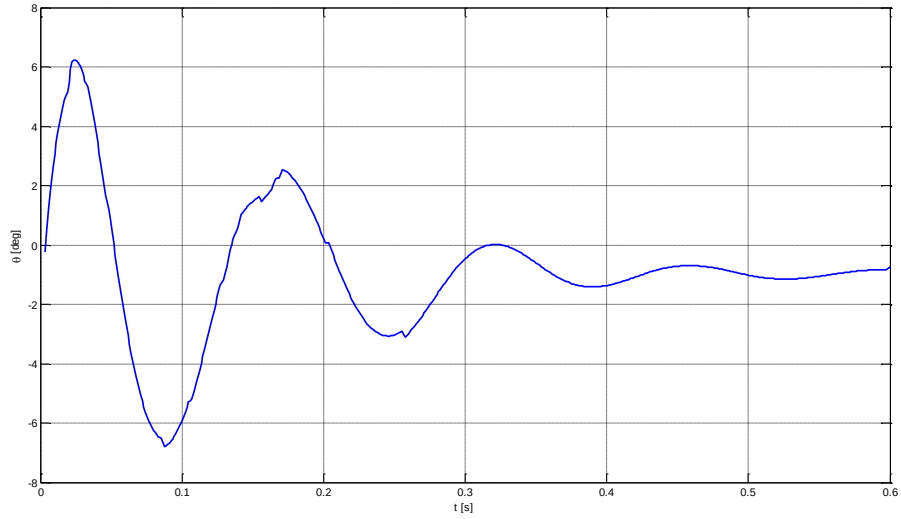

Figure 84: sensorless current control operation. Error angle with a step current reference equal to the rated current

5.3.3 Speed Control

On Simulink, the MRAS model works properly with every waveform speed reference, but with a real RSM, there a problem.
Whit a speed reference with a high amplitude the control injects a little current on the motor to keep a constant speed, due to the friction. If it is set a speed reference with a lower amplitude, the control, which works on the MTPA, passes for a very short time on the point where the injected current is equal to zero. This is sufficient to make a result to the vector product equal to zero. Having an error equal to zero the MRAS part thinks to estimate the correct speed and positon of the rotor, but rotor speeds tends to zero.

To solve this problem, when the current has a value equal to 0,5 A (this value has been found with different tests), the current control does not work on the MTPA, but it works in a pink line, like shown in Fig. 85.

Thanks to this idea, the vector product is zero only if the MRAS part it is estimating properly the speed and position of the rotor.

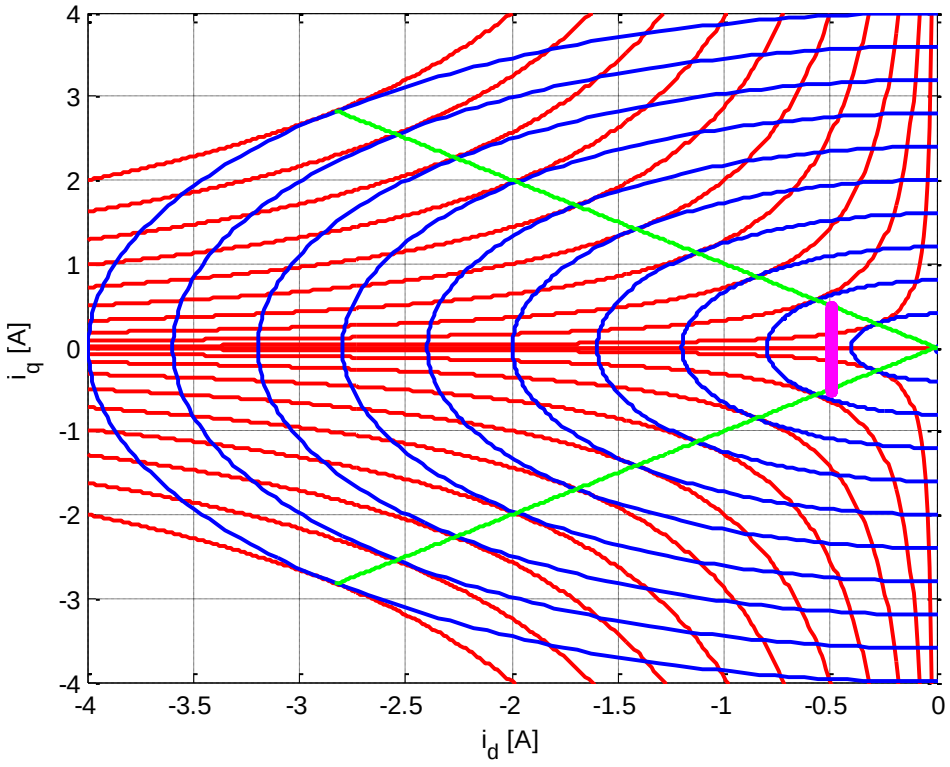

Figure 85: region of operation of the RSM with current limits (blue lines),torque lines (red lines), MTPA (green lines) and current control techique for the MRASmethod (magenta)

Fig. 86 shows the performance of the speed sensorless control. Whit the chosen values of the regulators coefficients, the speed has not overshoot and the rise time is approximately equal to 1,5 s.

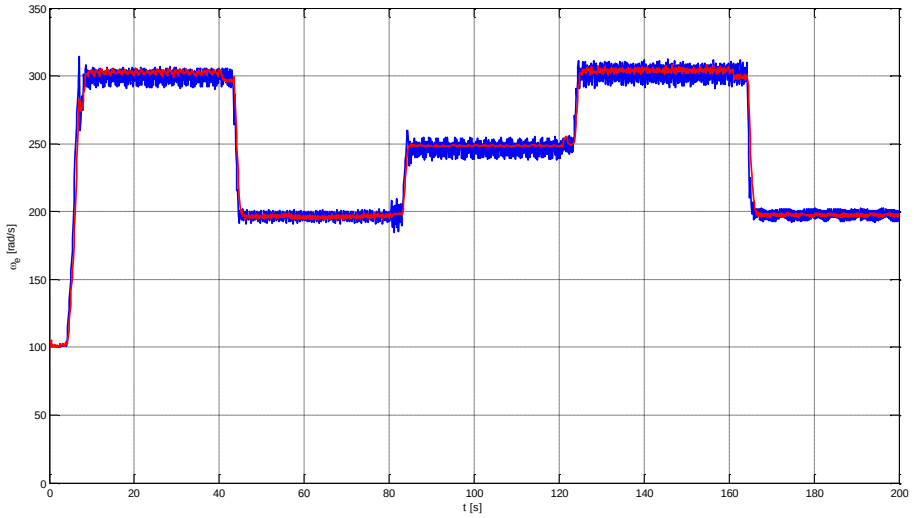

Figure 86: sensorless speed control operation. Measured (red) and estimated (blue) speeds with different step speed references

The MRAS program is developed to work in a speed range with amplitude from 100 rad/s until 300 rad/s.

6 . Conclusion

The master thesis explains the implementation of two sensorless controls: the high frequency method and the MRAS method. The first technique is used to estimate the initial position of the rotor and to realize a position and low speed sensorless control. The second technique is used to obtain a high and medium speed sensorless control. The thesis shows the result of the sensorless simulations and the obtained results with the implementations. With the combination of two methods it is possible to obtain complete sensorless control of the reluctance synchronous machine.

6.1 Summary of the thesis

In the follow list it is written the contents of the master thesis:

- Theory about the reluctance synchronous machine, the PI regulators and of the two sensorless control.
- Implementation of the HF and MRAS sensorless control simulations and their obtained results.
- Practical implementation of the HF and MRAS sensorless control and their obtained results.

All the obtained results show the high efficiency of these sensorless methods. In the reluctance synchronous machine, respect the other synchronous machines, the practical implementations results very difficult due to problems like the heavy saturation. Anyway, if these sensorless controls work properly with this type of electrical machine, their performance will be higher working in electrical machines, like the permanent magnets synchronous machines.

Appendix: Calculation of the RSM parameters

In the MRAS method, the adjustable model is obtained from the equations of the RSM. However, these equations depend from the RSM parameters, which are stator resistance and d and q axes inductances. To have a good MRAS estimators, it is important to find the right values of these parameters.

- **Stator resistance**

The stator resistance can be measured easily, supplying two RSM phases with a DC (direct voltage). Following, measuring the voltage between the two phases with a voltmeter and the injected current from the DC generator, it is possible to obtain the stator resistance value:

$$R = \frac{V_m}{2I_m}$$

where V_m is the measured voltage and I_m is the measured current.

The scheme is shown in Fig. 87.

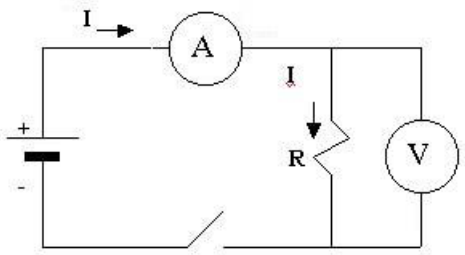

Figure 87: scheme to measure the stator resistance

- **Non ideal PWM inverter**

The non ideality of the PWM inverter is made to different causes, but the most notable is the dead-time. As to explain in the Chapter 2, the PWM inverter brakes a period in many smaller fractions, creating, in theory, a square control waveform

signal. In the reality, the voltage waveform is a ramp. This effect is not high when inverter works close to the maximum voltage for a lot of parts of the period, but having a RSM with a low power, which works with a low reference voltage during the tests it is necessary to estimate how this fact influences the "seen" resistance from the control and compensate it.

This is realized with the adjustable model shown in Fig. 45, where the *we* input is the measured speed by encoder. The rotor is locked lined on real d axis thanks to the IM, so if the d and q inductances are not estimated rightly, they will not give problems. After, the RSM is supplied before with only different d voltage values and after it is done the same process with the q voltage. For every value, voltages and currents are measured their ratio is the seen resistance. Now it is possible to write an equation to express these resistance values in function of the measured current

or of the measured voltage. It is chosen to express the resistance in function of the current. Dependence from resistance and current results the same for the d and q axes, it is shown in Fig. 88.

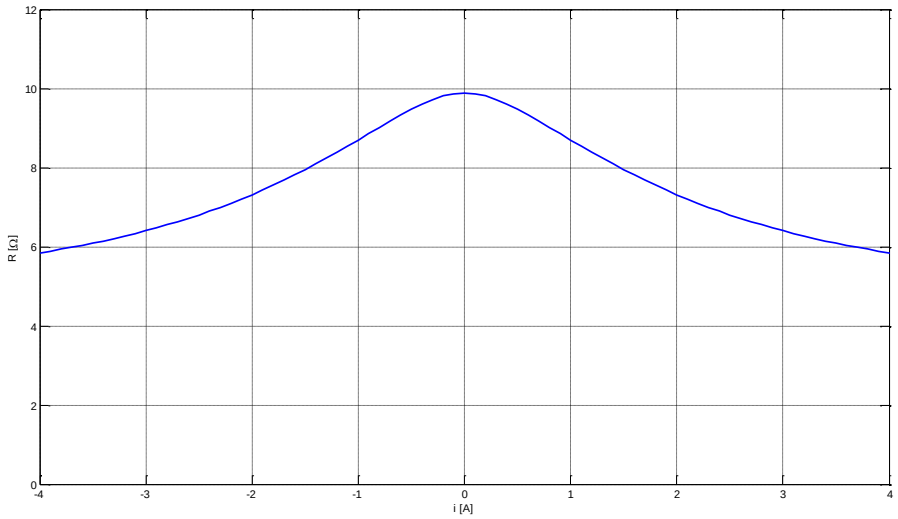

Figure 88: effect od the non-ideal PWM inverter

The function is:

$$R = 4{,}98 + 6{,}40e^{-|I|/2} - 1{,}5e^{-|I|/0{,}45}$$

- **d and q axes inductances**

The correct estimation the d and q inductances waveforms is important to control rightly the RSM with the MRAS method. The PMSMs are affected from the

inductances saturation, especially the RSMs. Following, it is explained three method to be sure to have estimated correctly the inductances waveforms.

Injection of a HF carrier vector

A HF carrier vector is injected in the RSM with the locked rotor and phase voltages and currents are saved. Their values have been elaborated in Matlab, realizing their FFT in stationary reference frame. The imaginary parts of the ratios of the voltage positive sequence with the current positive sequence and with the current negative sequence are equal to respectively average inductance and differential inductance. Now it is possible to know the inductances values.

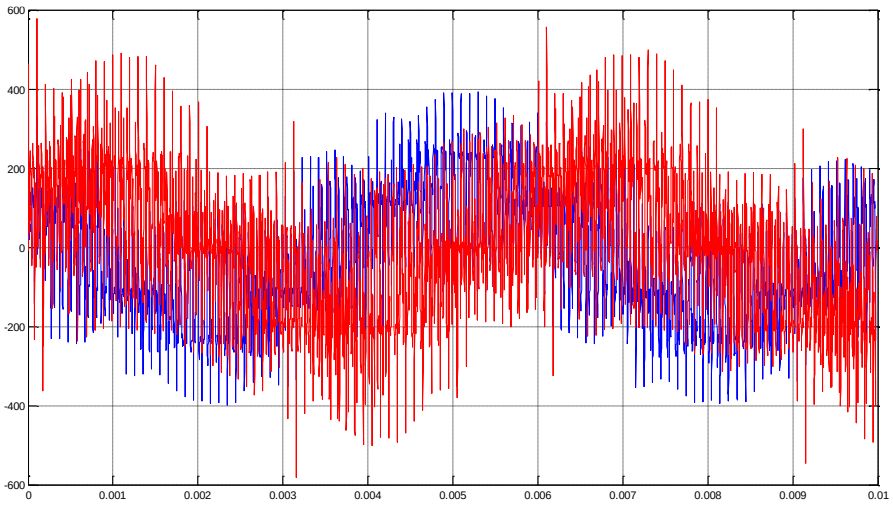

Figure 89: injected high frequency d (blue) and q (red) voltages. Vhf=150 V, ωhf=2*π*166 Hz

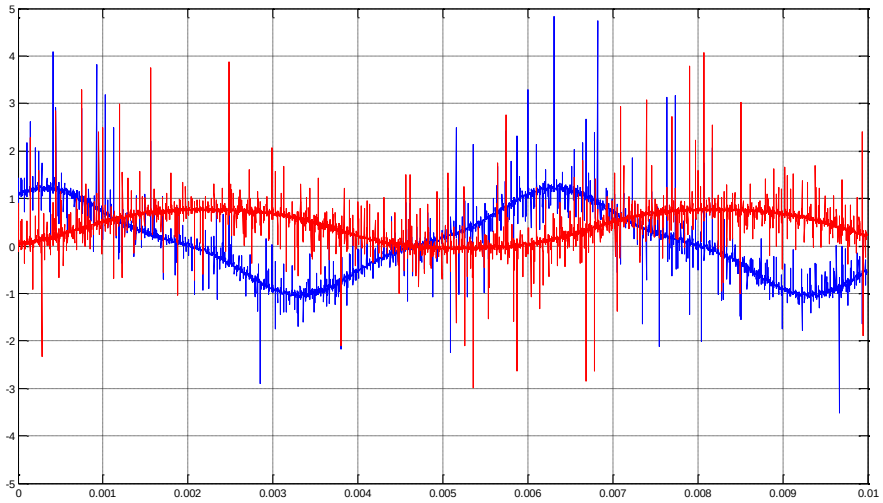

Figure 90: high frequency d (blue) and q (red) currents. Vhf=150 V, ωhf=2*π*166 Hz

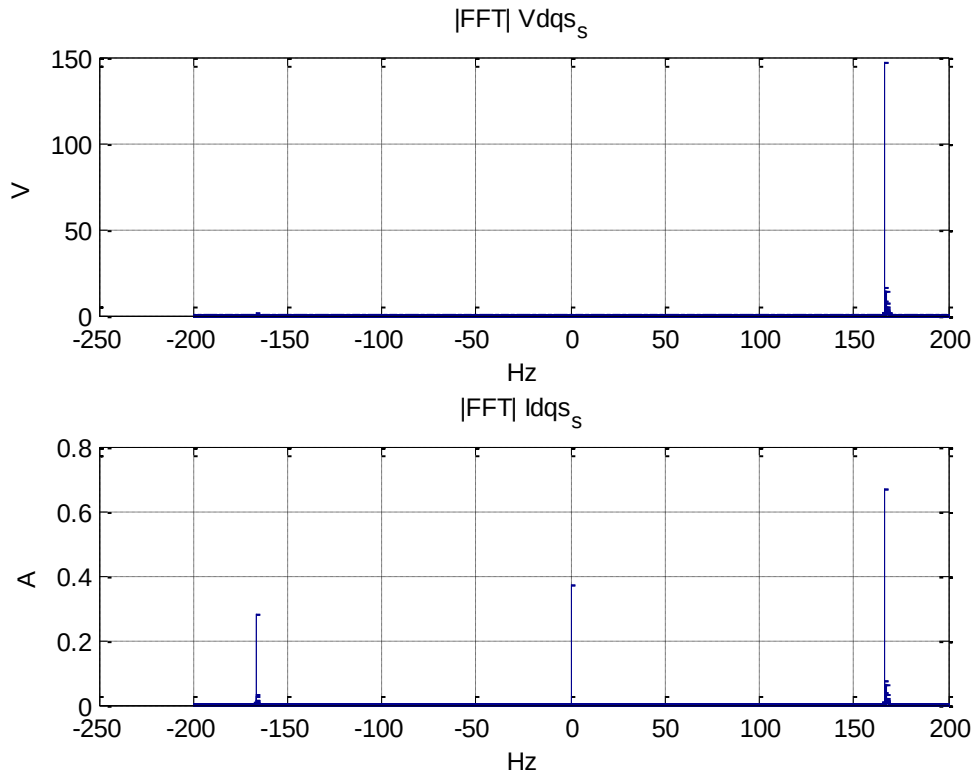

Figure 91: frequency spectrum of the injected high frequency voltage (top) and the resulting high frequency current (bottom). Vhf=150 V, ωhf=2*π*166 Hz

Another way to find the differential inductance is with the equation of the torque, knowing the nominal torque and current and the MTPA of the machine, the differential inductance results:

$$\Delta L = \frac{L_d - L_q}{2} = \frac{2\,m}{3\,p\,I_n^2}$$

Step voltage reference

Anyway to obtain the waveforms of the inductances, one way is to keep the rotor lined up with the real d axis thanks to the IM and to inject various step voltage references with different initial and final values, before in d axis and after in q axis. Saving the obtained current waveform, it is possible to approximate it with an exponential, where its time constant is equal to the ration between the wanted inductance and the stator resistance. Successively the equations that express the d and q inductances in function respectively of the d and q currents result:

$$L_d = 0{,}270 + 0.10e^{-|I|/2{,}5} + 0{,}01\left(1 - e^{-|I|/0{,}20}\right)$$
$$L_q = 0{,}088 + 0.15e^{-|I|/1{,}9} + 0{,}03\left(1 - e^{-|I|/0{,}35}\right)$$

Fig.s 92, 93, 94 show respectively the d and q inductances waveforms, the difference and ratio between d and q inductances

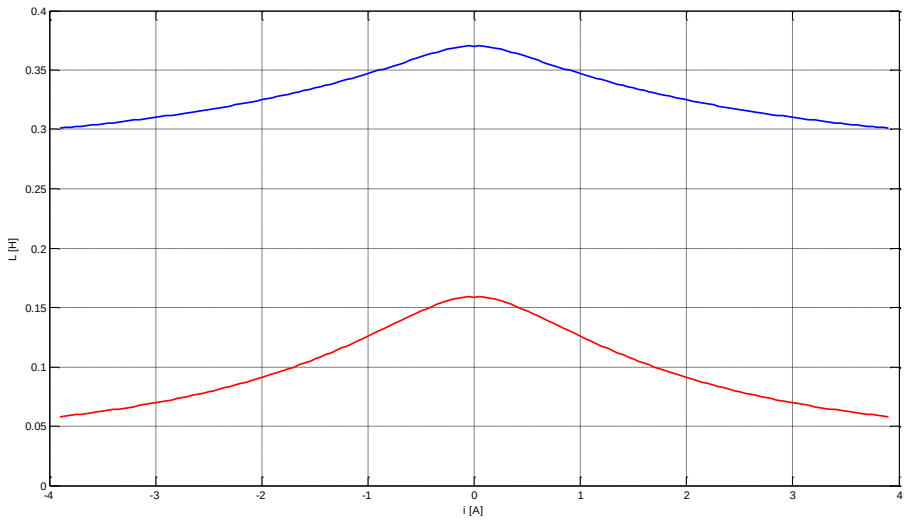

Figure 92: waveforms of d (blue) and q (red) inductances

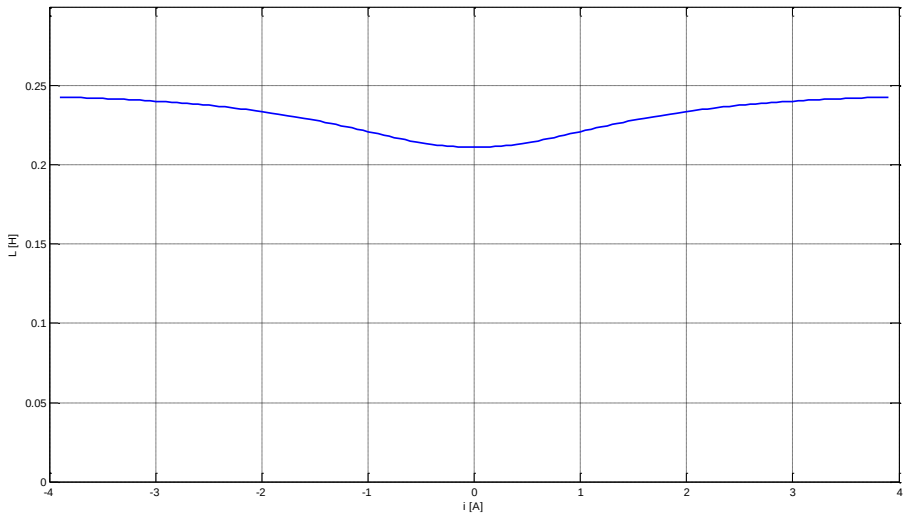

Figure 93: inductance value difference between d an q inductances

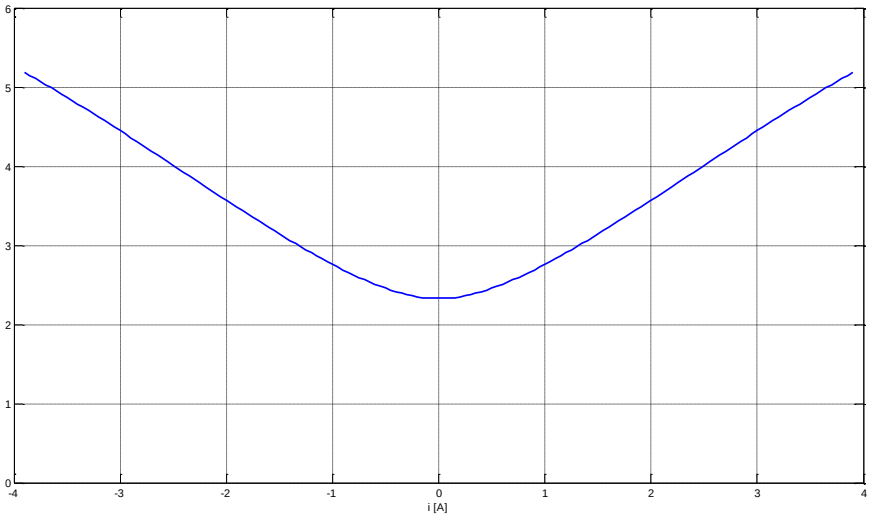

Figure 94: ratio between d and q inductances

In the MRAS part of the Chapter 5, it is shown the current control with the compensation. In Fig. 95 it is demonstrated the current sensorless control neglecting the compensation of the inductances.

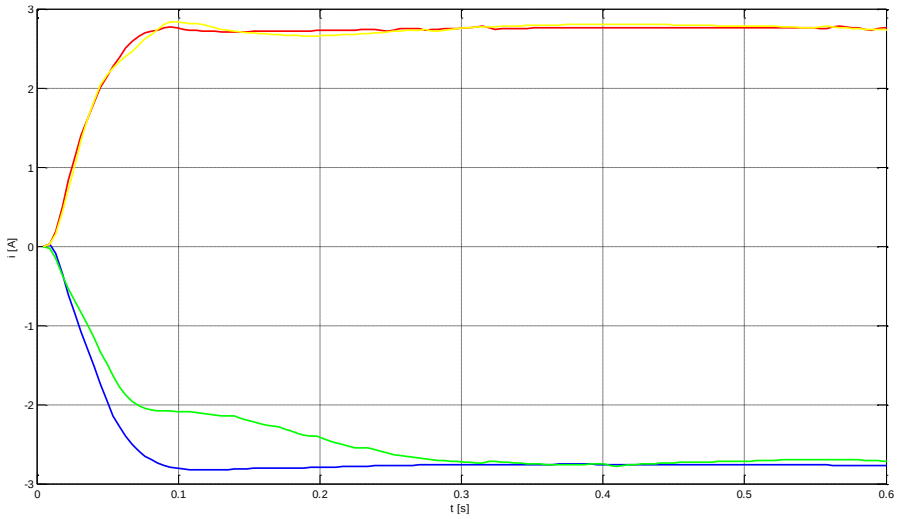

Figure 95: sensorless current control operation. Estmated d (green) and q (yellow) currents and measured d (blue) and q (red) currents with MRAS method without the compensation of the saturation

References

Publication 1: A. Kilthau and M. Pacas, “Parameter-measurement and control of the synchronous reluctance machine including cross saturation,” in Conf. Rec. IEEE IAS Annu. Meeting, Chicago, IL, 2001, pp. 2302–2309.

Publication 2: I. Boldea, L. Janosi, and F. Blaabjerg, “A modified direct torque control (DTC) of reluctance synchronous motor sensorless drive,” Electr. Mach. Power Syst., vol. 28, no. 2, pp. 115–128, 2000.

Publication 3: T. Matsuo and A. Lipo, “Rotor position detection scheme for synchro- nous reluctance motor based on current measurements,” IEEE Trans. Ind. Appl., vol. 31, no. 4, pp. 860–868, Jul./Aug. 1995.

Publication 4: H. W. De Kock, M. J. Kamper, and R. M. Kennel, “Anisotropy comparison of the reluctance and PM synchronous reluctance machines for position sensorless control using HF carrier injection,” IEEE Trans. Power Electron., vol. 24, no. 8, pp. 1905–1913, Aug. 2009.

Publication 5: L. A. de S. Ribeiro, M.C. Harke, and R.D. Lorenz, “Dynamic Properties of Back-emf Based Sensorless Drives,” IEEE-IAS’06, Vol. 4, pp. 2026 - 2033, Oct 2006.

Publication 6: P. P. Acarnely and j. F. Watson, “Review of Position-Sensorless Operation of Brushless Permanent-Magnet Machines,” IEEE Trans. Ind. Electron., vol. 53 (2), pp.352-362, Apr. 2006.

Publication 7: M. Schroedl, “Sensorless control of AC machines at low speed and standstill based on the ‘INFORM’ method,” IEEE-IAS’96, vol. 1, pp. 270–277, 1996.

Publication 8: S. Ogasawara and H. Akagi, "Approach to real-time position estimation at zero and low speed for a PM motor based on saliency," IEEE Trans. Ind. Applicat., vol. 34, pp. 163-168, Jan.-Feb. 1998.

Publication 9: J. Holtz and H. Pan, “Acquisition of rotor anisotropy signals in sensorless position control systems,” IEEE Trans. Ind. Appl., Sept./Oct. 2004, Vol. 40 (5), pp. 1379–1387.

Publication 10: C. Blanco, D. D. Reigosa, F. Briz and J. M. Guerrero, “Synchronization in higly distorted three-phase grids using selective nothc filters”, IEEE Electron.

Publication 11: Wei-Hua Li, Zi-Zing Chen, Wen-Ping Cao, “Simulation research on optimization of permanent magnet synchronous motor sensorless vector control based on MRAS”, IEEE, pp. 350-355.

Publication 12: G. Ahmad, H. Tsuyoshi, “Very low speed sensorless vector control of synchronous reluctance motors with a novel startup scheme”, IEEE, pp. 396-402.

Publication 13: S. Ichikawa, M. Tomita, S. Doki, S. Okuma, “Novel model od synchronous reluctance motors including magnetic saturation and its sensorless control”, IEEE, pp. 1213-1218.

Publication 14: A. Faggion, S. Bolognani, N. Bianchi, “Ringed-pole permanent magnet synchronous motor for position sensorless drives”, IEEE, pp. 3837-3844.

Publication 15: D. D. Reigosa, P. Garcia, F. Briz, D. Raca, R. D. Lorenz, “Modeling and adaptive decoupling of transient resistance and temperature effects in carrier-based sensorless control of PM synchronous machines”, IEEE, pp. 1-8.

Publication 16: D. Raca, P. Garcia, D. D. Reigosa, F. Briz, R. D. Lorenz, “Carrier signal selection for sensorless control of PM synchronous machines at zero and very low speeds”, IEEE, p. 1-8.

Publication 17: F. Briz, A. Diez, M. W. Degner, “Dynamic operation of carrier signal injection based sensorless direct field-oriented AC drives”, IEEE, pp. 1360-1368.

Publication 18: C. Y. Yu, J. Tamura, D. D. Reigosa, R. D. Lorenz, “Position self-sensing evaluation of a FI-IPMSM based on high-frequrncy signal injiection methods”, IEEE, pp.880-888.

Publication 19: M. Nagrial, J. Rizk, A. Hellany, “Analisys and performance of high efficiency synchronous reluctance machines”, IEEE, pp.247-254.

Publication 20: P. Garcia, J. M. Guerrero, F. Briz, D. D. Reigosa, “Sensorless control of three-pole active magnetic bearings using saliency-tracking-based methods”, IEEE, pp. 1476-1484.

Publication 21: D. Raca, D. D. Reigosa, F. Briz, R. D. Lorenz, “A comparative analisys of pulsating vs. rotating vector carrier signal injection-based sensorless control”, IEEE, pp. 879-885.

Publication 22: A. Piippo, J. Luomi, “Adaptive observed combined with HF signal injection for sensorless control of PMSM drives”, IEEE, pp. 674-681.